

# Algebraic multigrid methods for saddle point systems arising from mortar contact formulations

T. A. Wiesner<sup>1,‡</sup>, M. Mayr<sup>2,\*</sup>, A. Popp<sup>2,‡</sup>, M. W. Gee<sup>3</sup> and W. A. Wall<sup>4</sup>

<sup>1</sup> Leica Geosystems AG, Heinrich-Wild-Strasse 201, 9435 Heerbrugg, Switzerland

<sup>2</sup> Institute for Mathematics and Computer-Based Simulation, Universität der Bundeswehr München, Werner-Heisenberg-Weg 39, D-85577 Neubiberg, Germany

<sup>3</sup> Mechanics & High Performance Computing Group, Technische Universität München, Parkring 35, D-85748 Garching, Germany

<sup>4</sup> Institute for Computational Mechanics, Technische Universität München, Boltzmannstr. 15, D-85748 Garching, Germany

## SUMMARY

In this paper, a fully aggregation-based algebraic multigrid strategy is developed for nonlinear contact problems of saddle point type using a mortar finite element approach. While the idea of extending multigrid methods to saddle point systems is not new and can be found, e.g., in the context of Stokes and Oseen equations in literature, the main contributions of this work are (i) the development of an interface aggregation strategy specifically suited for generating Lagrange multiplier aggregates that are required for coupling structural equilibrium equations with contact constraints and (ii) an analysis of saddle point smoothers in the context of constrained interface problems. The proposed method is simpler to implement, computationally less expensive than the ideas from [1], and – in the authors' opinion – the presented approach is more intuitive for contact problems. The new interface aggregation strategy perfectly fits into an aggregation-based multigrid framework and can easily be combined with segregated transfer operators, which allow to preserve the saddle point structure on the coarse levels. Further analysis provides insight into saddle point smoothers applied to contact problems, while numerical experiments illustrate the robustness of the new method.

Received ...

**KEY WORDS:** Algebraic multigrid methods, Contact mechanics, Mortar methods, Iterative linear solvers, Preconditioning

## 1. INTRODUCTION

Many engineering applications require the simulation of large-scale contact problems. Therefore, it is not surprising that recent years have seen significant progress in modelling and simulation of contact interaction and its associated phenomena, such as friction [24, 46, 59], wear [12, 20, 39, 42], adhesion [40, 58], or multi-scale contact phenomena [6, 66]. This is particularly true with regard to robust finite element based discretization techniques for finite deformations and efficient nonlinear solution algorithms. Above all, mortar finite element methods — originally introduced in the context of domain decomposition [2, 5] — are meanwhile well-established as a basis for state-of-the-art contact formulations and widely accepted among researchers as being superior to more classical discretization techniques, such as the the node-to-segment (NTS) method, the Gauss-point-to-segment (GPTS) method and other collocation based approaches [17, 52, 53, 82, 85].

\*Correspondence to: M. Mayr, Institute for Mathematics and Computer-Based Simulation, Universität der Bundeswehr München, Werner-Heisenberg-Weg 39, D-85577 Neubiberg, Germany, E-mail: matthias.mayr@unibw.de

‡This work was partially performed while these authors were affiliated with the Institute for Computational Mechanics, Technische Universität München, Boltzmannstr. 15, D-85748 Garching, Germany.

Nowadays, constraint enforcement in the context of mortar methods is often based on a regularized Lagrange multiplier scheme or an augmented Lagrange method instead of a simple, yet often insufficient penalty approach. Independent from the actual details of the constraint enforcement implementation, the discrete Lagrange multipliers constitute an additional set of degrees of freedom in the mortar finite element contact formulation. When using a dual mortar approach [29, 32, 33, 48, 50, 80, 81], the discrete Lagrange multiplier basis is chosen based on a biorthogonality condition with the underlying finite element basis. This allows for the localization of the contact constraints and, thus, from a more algebraic point of view, for the trivial condensation of the additional Lagrange multiplier degrees of freedom from the final linearized systems of equations. If such a static condensation is not desired or not feasible (e.g. when choosing a standard basis rather than dual basis functions for the Lagrange multipliers, see e.g. [47, 81]), the linear system remains in its generalized saddle point format arising from the contact constraint equations. Both the standard and the dual mortar approach have become increasingly popular in recent years, with new contributions focusing for example on higher-order finite element interpolation [49, 83], isogeometric mortar methods [16, 60, 62, 63, 86], or improved robustness of the solution algorithms [21, 30, 51], to name only a few particularly active research directions.

It is striking, however, that almost all current research endeavors concerned with mortar finite element methods for contact mechanics focus exclusively on the modelling of various contact phenomena. Yet, for large-scale and industrial applications the appropriate modelling of contact problems is not sufficient. In fact, the demand for efficient solution strategies tailored to the specifics of contact simulations is eminent in order to achieve optimal over-all performance. Whereas one could use parallel direct solvers to solve the linear systems, they are not an option for very large problems. Iterative solvers for sparse systems (e.g. [27, 56]) combined with good preconditioning strategies are a far better choice with respect to computational resources. In particular, multigrid methods [28, 65] are known to be among the most efficient solution and preconditioning strategies, at least for certain classes of problems.

From the perspective of the linear solvers and multigrid-based preconditioners, the condensation of the Lagrange multipliers seems to be very attractive, since it allows to circumvent the more-sophisticated saddle point formulation. For contact problems though, we have experienced that the resulting linear systems after condensation suffer from some challenging matrix properties which cause severe convergence problems for standard preconditioning techniques. In particular, the matrices tend to be non-diagonally dominant due to different (local) coordinate systems that are typically used for the formulation of the structural equilibrium equations and the contact constraints. In our previous work [78], we have developed multilevel preconditioners that address such issues and are specifically tailored to contact problems using the dual mortar method in a condensed formulation.

On the other hand, multigrid methods already have been successfully applied to saddle point problems as they arise from different applications (e.g. Stokes flow [34] or incompressible Navier-Stokes problems [26, 41]) and even in the context of mortar finite element methods [76, 79]. The multigrid theory for this particular class of saddle point problems has evolved starting from special multigrid methods for mortar finite element methods (e.g. [8, 25, 36, 84]) to mortar finite element methods in saddle point formulation (e.g., [9, 10]). Based on these ideas, specific multigrid methods for contact problems in saddle point formulation have been developed in [75]. However, most of the literature available on multigrid for mortar finite element methods and contact problems in saddle point formulations is primarily on geometric multigrid methods with abundant work on saddle point smoothers (cf. [89]). A first algebraic multigrid method for mortar-based contact problems has been proposed by Adams [1], performing standard aggregation on the graph of an auxiliary matrix imitating the Lagrange multipliers.

In this paper, we address the case of mortar-based contact problems in saddle point formulation and show how to tailor iterative solvers with algebraic multigrid preconditioners to such problems. In contrast to geometric multigrid methods, algebraic multigrid methods (e.g. [61]) do not rely on geometric user-provided mesh information, but use only purely algebraic information from the fine level matrix. Since static condensation of Lagrange multiplier unknowns is not required, our approach is applicable to mortar methods using both standard or dual shape functions. The proposed multigrid method is based on the (smoothed) aggregation algebraic multigrid algorithms (cf. [57, 68, 69, 71, 72]) with special extensions for block matrices and some minor contact-specific adaptions. We propose a novel aggregation strategy for the discrete Lagrange multiplier unknowns along the contact interface. Along with segregated transfer operators suitable for block matrices, we then can transfer the contact constraints to all coarse levels. We analyze various Schur complement block smoothers and assess their suitability for satisfying the contact constraints. Finally, we demonstrate and assess the performance of the proposed preconditioner in several three-dimensional examples.

The remainder of this paper is organized as follows: Section 2 provides a brief introduction to mortar methods for finite deformation contact problems in saddle point formulation. After the basic notation is introduced, we specifically present the resulting linear system that is arising if the discrete Lagrange multipliers are explicitly included into the set of unknowns to be solved for. After a brief introduction to the general idea of multigrid methods, Section 3 describes our strategy to tailor a multigrid preconditioner to contact problems in saddle point formulation. It comprises the coarsening of the mortar contact constraints as detailed in Section 4 as well as suitable block smoothers as discussed in Section 5. Finally, Section 6 presents numerical examples that showcase the robustness of the proposed multigrid preconditioners, before we close with some final remarks.

## 2. MORTAR METHODS FOR FINITE DEFORMATION CONTACT

As this paper is concerned with preconditioning of the system of linear equations arising from contact problems, just a brief summary to the contact formulation and discretization is given here. For a detailed presentation, the reader is referred to our previous work [48].

### 2.1. Problem formulation and governing equations

We consider two solid bodies, which are represented by  $\Omega_0^{(1)}, \Omega_0^{(2)} \subset \mathbb{R}^d$  with  $d \in \{2, 3\}$  in the reference configuration. Their surfaces  $\partial\Omega_0^{(i)}, i \in \{1, 2\}$  are decomposed into three disjoint subsets  $\Gamma_D^{(i)}, \Gamma_N^{(i)}$  and  $\Gamma_C^{(i)}$  denoting the Dirichlet boundary, the Neumann boundary, and the potential contact interface with unknown contact tractions  $\mathbf{t}_C^{(i)}$ , respectively. The solid bodies themselves are governed by nonlinear elasticity. Since we are only interested in the algebraic block structure of the final system of equations after discretization and linearization, it is sufficient to discuss a quasi-static contact problem with only two deformable bodies.

In order to describe the contact phenomenon, we state the Hertz-Signorini-Moreau conditions

$$g_n \geq 0 \quad \wedge \quad p_n \leq 0 \quad \wedge \quad g_n p_n = 0. \quad (1)$$

Therein,  $g_n$  defines a so-called gap function, which measures the distance of a point on the slave interface  $\gamma_C^{(S)}$  to the projected corresponding point on the master side  $\gamma_C^{(M)}$  of the contact interface in the current configuration. In the mathematical formulation, one introduces the negative slave side contact traction  $\mathbf{t}_C^{(1)}$  as Lagrange multiplier, i.e.,  $\boldsymbol{\lambda} = -\mathbf{t}_C^{(1)}$ . Using  $\mathbf{n}$  to denote the outward unit normal vector, the normal part of the contact stress can be denoted by  $\lambda_n := \boldsymbol{\lambda}^\top \mathbf{n}$  and the tangential part by  $\lambda_\tau := \boldsymbol{\lambda} - \lambda_n \mathbf{n}$ .

We employ the usual function spaces  $\mathcal{U}^{(i)}$  and  $\mathcal{V}^{(i)}$  for the displacement field  $\mathbf{u}$  of the the solid body and its weighting function  $\mathbf{v}$ , respectively. Furthermore, a suitable function space  $\mathcal{M}_+$  for the Lagrange multiplier field  $\boldsymbol{\lambda}$  and its weighting function  $\boldsymbol{\mu}$  is assumed. The weak form of the governing equations then reads: Find  $(\mathbf{u}, \boldsymbol{\lambda}) \in \mathcal{U} \times \mathcal{M}_+$  such that

$$-\delta\mathcal{W}_{\text{int,ext}} + \int_{\gamma_C^{(S)}} \boldsymbol{\lambda} (\mathbf{v}^{(1)} - \mathbf{v}^{(2)}) \, dA = 0, \quad \forall \mathbf{v} \in \mathcal{V}, \quad (2a)$$

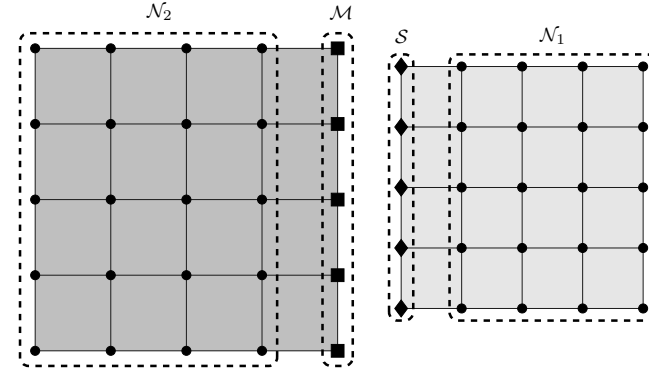
$$\int_{\gamma_C^{(S)}} (\mu_n - \lambda_n) g_n \, dA \geq 0, \quad \forall \boldsymbol{\mu} \in \mathcal{M}_+. \quad (2b)$$

Herein, the internal and external virtual work contributions  $\delta\mathcal{W}_{\text{int,ext}}$  are defined as usual in nonlinear solid mechanics (cf. [47, 88]) and, thus, further details are omitted. The second term in (2a) can be identified as contact virtual work  $\delta\mathcal{W}_c$  and the expression in (2b) as variational inequality formulation of the contact constraints. An extension to frictional contact based on Coulomb's law is straightforward and can be found in our previous work [24] for example.

### 2.2. Finite element discretization

For spatial discretization of the displacement field, either isoparametric finite elements with first-order and second-order Lagrange interpolation or isogeometric analysis (IGA) with NURBS-based shape functions are employed. After discretization, the discrete representation of displacement unkowns is given by the nodal degrees of freedom (DOFs)

$$\mathbf{u} = [\mathbf{u}_{\mathcal{N}_1}, \mathbf{u}_{\mathcal{S}}, \mathbf{u}_{\mathcal{M}}, \mathbf{u}_{\mathcal{N}_2}]^\top.$$



- Inner nodes with displacement degrees of freedom  $\mathbf{u}_{\mathcal{N}_1} \in \Omega_0^{(1)} \setminus \Gamma_c^{(1)}$  and  $\mathbf{u}_{\mathcal{N}_2} \in \Omega_0^{(2)} \setminus \Gamma_c^{(2)}$
- ◆ Nodes at slave contact interface  $\Gamma_c^{(S)} = \Gamma_c^{(1)}$  with displacement degrees of freedom  $\mathbf{u}_A$  and  $\mathbf{u}_I$
- Nodes at master contact interface  $\Gamma_c^{(M)} = \Gamma_c^{(2)}$  with displacement degrees of freedom  $\mathbf{u}_M$

Figure 1. Schematic mesh illustrating interior, master and slave interface nodes.

Therein, the  $\mathbf{u}_{\mathcal{N}_i}$ ,  $i \in \{1, 2\}$ , contain all degrees of freedom associated with the mesh nodes of the corresponding solid body without the nodes at the contact interface, where we use the convention that indices 1 and 2 denote the slave and master “body”, respectively. The degrees of freedom associated with the contact interface on the slave and master side are represented by  $\mathbf{u}_S$  and  $\mathbf{u}_M$ , respectively.

Since (2) represents a mixed variational form, we also have to discretize the Lagrange multiplier field  $\boldsymbol{\lambda}$ . We choose to follow a mortar approach for its mathematical properties and its superiority to other schemes [17, 52, 53, 82, 85]. As usual for mortar methods, the Lagrange multiplier field is discretized on the slave side contact interface  $\gamma_c^{(S)}$  in the current configuration. We either use standard ansatz functions, i.e. Lagrange polynomials with a trace space relation with the underlying volume element, or dual shape functions. The latter satisfy a biorthogonality property and, thus, allow for a computationally cheap condensation of the additional unknown Lagrange multipliers from the final system of equations. For details on dual basis functions in the context of mortar-based contact discretizations, we refer to [37, 49, 81]. Their interplay with preconditioners for iterative linear solvers has been discussed in our previous work [78]. The vector of discrete Lagrange multipliers is now referred to as  $\boldsymbol{\lambda}$ . A schematic mesh illustrating interior, slave interface, and master interface nodes is sketched in Figure 1.

The final spatially discretized formulation of the quasi-static frictionless problem (2) using the nodal vector representation now emerges as

$$\mathbf{f}_{\text{int}}(\mathbf{u}) + \mathbf{f}_{\text{co}}(\mathbf{u}, \boldsymbol{\lambda}) = \mathbf{f}_{\text{ext}}, \quad (3a)$$

$$(\tilde{g}_{n,h})_j \geq 0, \quad (\lambda_n)_j \geq 0, \quad (\tilde{g}_{n,h})_j (\lambda_n)_j = 0, \quad j = 1, \dots, n^{(S)}, \quad (3b)$$

$$(\boldsymbol{\lambda}_\tau)_j = \mathbf{0}, \quad j = 1, \dots, n^{(S)}. \quad (3c)$$

The internal forces  $\mathbf{f}_{\text{int}}(\mathbf{u})$  and external forces  $\mathbf{f}_{\text{ext}}$  are common in nonlinear finite element methods and need no further explanation. The discrete vector of contact forces  $\mathbf{f}_{\text{co}}$  is computed based on two mortar matrices  $D$  and  $M$ , arising from the integral over the slave interface  $\gamma_c^{(S)}$  in (2a), and the discrete Lagrange multiplier vector  $\boldsymbol{\lambda}$ . For details regarding the computation of  $D$  and  $M$ , see [48, 52] for example. Finally, a closer look at the discrete contact constraints reveals that (3b) basically represents a discrete version of the Karush–Kuhn–Tucker (KKT) type conditions in (1) with an additional weighting based on the Lagrange multiplier shape functions  $\psi_j$ , while the nodal enforcement of frictionless sliding in (3c) is straightforward anyway.

Since the discrete contact constraints summarized in (3b) are still formulated as inequalities, an active set strategy usually referred to as primal-dual active set strategy (PDASS) is needed in addition to the usual nonlinear solution procedure to identify the currently active and inactive contact regions  $\mathcal{A}$  and  $\mathcal{I} = \mathcal{S} \setminus \mathcal{A}$ , respectively. It has been demonstrated in [13, 31, 54] that the PDASS can equivalently be interpreted as a semi-smooth Newton method, thus allowing for an integrated treatment of all

nonlinearities (including the search for the active set) within one single Newton–Raphson type iteration loop. Meanwhile, many successful applications to small and large deformation contact problems can be found in the literature [24, 32, 33, 48].

### 2.3. Algebraic formulation of linear systems

For efficient iterative solution strategies based on multigrid methods for nonlinear contact problems, one is primarily interested in the structure of the linear systems arising in each nonlinear iteration step of the underlying Newton–Raphson scheme. For the sake of brevity, details on the linearization process and on the Newton–Raphson procedure are omitted here and the interested reader is instead referred to [48, 50].

Consistent linearization of (3) and a subsequent update of the active set  $\mathcal{A}$  and inactive set  $\mathcal{I}$  yields the system

$$\left( \begin{array}{cccccc|cc} K_{\mathcal{N}_1\mathcal{N}_1} & K_{\mathcal{N}_1\mathcal{M}} & 0 & 0 & 0 & 0 & 0 \\ K_{\mathcal{M}\mathcal{N}_1} & K_{\mathcal{M}\mathcal{M}} & K_{\mathcal{M}\mathcal{I}} & K_{\mathcal{M}\mathcal{A}} & 0 & -M_{\mathcal{I}}^T & -M_{\mathcal{A}}^T \\ 0 & K_{\mathcal{I}\mathcal{M}} & K_{\mathcal{I}\mathcal{I}} & K_{\mathcal{I}\mathcal{A}} & K_{\mathcal{I}\mathcal{N}_2} & D_{\mathcal{I}\mathcal{I}}^T & D_{\mathcal{I}\mathcal{A}}^T \\ 0 & K_{\mathcal{A}\mathcal{M}} & K_{\mathcal{A}\mathcal{I}} & K_{\mathcal{A}\mathcal{A}} & K_{\mathcal{A}\mathcal{N}_2} & D_{\mathcal{A}\mathcal{I}}^T & D_{\mathcal{A}\mathcal{A}}^T \\ 0 & 0 & K_{\mathcal{N}_2\mathcal{I}} & K_{\mathcal{N}_2\mathcal{A}} & K_{\mathcal{N}_2\mathcal{N}_2} & 0 & 0 \\ \hline 0 & 0 & 0 & 0 & 0 & 1 & 0 \\ 0 & N_{\mathcal{M}} & N_{\mathcal{I}} & N_{\mathcal{A}} & 0 & 0 & 0 \\ 0 & 0 & F_{\mathcal{I}} & F_{\mathcal{A}} & 0 & 0 & T_{\mathcal{A}} \end{array} \right) \begin{bmatrix} \Delta u_{\mathcal{N}_1} \\ \Delta u_{\mathcal{M}} \\ \Delta u_{\mathcal{I}} \\ \Delta u_{\mathcal{A}} \\ \Delta u_{\mathcal{N}_2} \\ \Delta \lambda_{\mathcal{I}} \\ \Delta \lambda_{\mathcal{A}} \end{bmatrix} = - \begin{bmatrix} r_{\mathcal{N}_1}^u \\ r_{\mathcal{M}}^u \\ r_{\mathcal{I}}^u \\ r_{\mathcal{A}}^u \\ r_{\mathcal{N}_2}^u \\ r_{\mathcal{I}}^{\lambda} \\ r_{\mathcal{A}}^{\lambda} \\ r_{\mathcal{A},\tau}^{\lambda} \end{bmatrix} \quad (4)$$

to be solved in every nonlinear iteration. Therein, the typical mortar matrices  $D$  and  $M$  together with the discrete Lagrange multipliers represent the discrete contact forces. In case of dual shape functions, the matrix  $D$  reduces to a diagonal matrix and, thus, allows for a cheap condensation of the Lagrange multiplier unknowns. Algebraic multigrid preconditioners for this type of condensed system have been proposed in our earlier paper [78]. Furthermore, matrices  $N_{\mathcal{M}}$ ,  $N_{\mathcal{I}}$ , and  $N_{\mathcal{A}}$  denote the linearizations of the weighted gap function of (3b) at all active contact nodes. Finally, linearizations of the frictionless sliding condition (3c) are referred to by matrices  $F_{\mathcal{I}}$ ,  $F_{\mathcal{A}}$ , and  $T_{\mathcal{A}}$ , respectively.

The  $2 \times 2$  block matrix indicated by the dashed lines in (4) describes a linear system with a typical generalized saddle point structure. The upper left block consists of the entries of the tangential stiffness matrix (i.e. linearized internal forces) as well as linearizations of contact forces w.r.t. displacement degrees of freedom  $u$  and the upper right block contains the linearizations of the contact forces w.r.t. the Lagrange multiplier unknowns  $\lambda$ . The distinct pattern of zero entries in this upper left block reveals that the two solid bodies (indices  $\mathcal{N}_1$  and  $\mathcal{N}_2$ ) are indeed only coupled through the slave and master sides of the contact interface (indices  $\mathcal{S}$  and  $\mathcal{M}$ ). Even though formulated for two solid bodies, the generalization to  $n$  solid bodies is straightforward and only a matter of notation. The upper right block represents the discrete contact operator  $C(u)$ , i.e. basically the two mortar matrices  $D$  and  $M$ . The very simple sixth block row emerges from (3b) and (3c) for inactive nodes.

Note that the given matrix has 8 block rows but only 7 block columns in our notation in order to emphasize that the normal and tangential parts of the contact constraints for active nodes are considered separately, i.e. these two rows contain consistent linearizations of the active branch of (3b) and of (3c). Again, we point out that this separate notation is possible due to the fact that a local convective coordinate system is employed for evaluating the contact constraints / Lagrange multiplier weights  $\mu$ , while the standard Cartesian frame is still applied for the discrete Lagrange multiplier values  $\lambda$  as well as the displacement unknowns. Yet, of course, the system matrix remains a square matrix with the total numbers of rows and columns being identical. The discrete vector  $g_{\mathcal{A}}$  contains all weighted gap values  $(\tilde{g}_{n,h})_j$  associated with the active nodes at the contact interface.

For ease of notation, the following short block notation is used in the remainder of the manuscript:

$$\begin{pmatrix} K & C_1^T \\ C_2 & -Z \end{pmatrix} \begin{bmatrix} \Delta u \\ \Delta \lambda \end{bmatrix} = - \begin{bmatrix} r^u \\ r^{\lambda} \end{bmatrix}. \quad (5)$$

## 3. MULTIGRID SCHEME FOR CONTACT PROBLEMS IN SADDLE POINT FORMULATION

Although multigrid methods can be used as standalone solvers for linear systems, they are usually incorporated into an iterative linear solver as a preconditioning method. Throughout this paper, we use a preconditioned generalized minimal residual (GMRES) solver [55] with one multigrid V-cycle sweep for preconditioning. A general introduction into the idea of preconditioning is beyond the scope of this paper. The reader is referred to the literature, e.g. [3].

MGV( $\mathbf{A}^{(\ell)}, x, b, \ell$ ):

if  $\ell \neq \ell_{max}$

$x \leftarrow \mathcal{S}_\ell^{\nu_1}(\mathbf{A}^{(\ell)}, x, b)$

$r \leftarrow b - \mathbf{A}^{(\ell)}x$

$c \leftarrow 0$

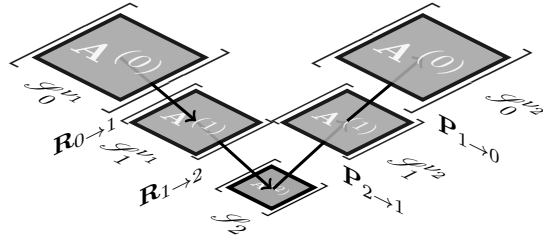
$c \leftarrow \text{MGV}(\mathbf{A}^{(\ell+1)}, x_{\ell+1}, \mathbf{R}_{\ell+1}r, \ell+1)$

$x \leftarrow x + \mathbf{P}_{\ell+1}c$

$x \leftarrow \mathcal{S}_\ell^{\nu_2}(\mathbf{A}^{(\ell)}, x, b)$

else  $x \leftarrow (\mathbf{A}^{(\ell)})^{-1}b$

(a) Recursive multigrid algorithm.



(b) Multigrid V-cycle in a 3 level setting.

Figure 2. Multigrid algorithm and V-cycle.

### 3.1. Algebraic multigrid methods in a nutshell

Multigrid methods are based on the finding that many well-known and computationally cheap iterative methods (e.g. relaxation based iterative methods such as Jacobi or Gauss-Seidel methods) to solve linear systems  $\mathbf{A}x = b$  effectively damp the high frequency part of an error vector but are less effective in damping out the low frequency error modes. Multigrid methods heavily make use of this smoothing property by applying such cheap smoothing methods on different resolutions of the fine level problem.

**3.1.1. Basic multigrid cycle and algorithm** The multigrid algorithm given in Figure 2a is briefly described as follows: on each multigrid level  $\ell$ , a level smoothing algorithm  $\mathcal{S}_\ell$  performs  $\nu_1$  pre-smoothing sweeps before the residual vector  $r$  is transferred to the next coarser level  $\ell+1$  using the restriction operator  $\mathbf{R}$ . After the coarse level problem has been solved on the coarsest level, the correction  $c$  is then prolongated using the prolongation operator  $\mathbf{P}$  and the solution vector is smoothed using  $\nu_2$  post-smoothing sweeps. Figure 2b illustrates this basic multigrid V-cycle, exemplifying a three-level setting. As one can see from Figure 2b, applying a multigrid method basically means applying level smoothers on coarse representations  $\mathbf{A}_\ell$  of the fine level problem  $\mathbf{A}_0$ .

**3.1.2. Algebraic multigrid methods** There are different strategies for defining the transfer operators  $\mathbf{P}$  and  $\mathbf{R}$  which are necessary to generate coarse level matrices  $\mathbf{A}_\ell$  ( $\ell > 0$ ). For algebraic multigrid (AMG), the fine level operator  $\mathbf{A}_0$  is sufficient to generate coarse level matrices  $\mathbf{A}_\ell$ . An important class of AMG is given with the *smoothed aggregation AMG* which is based on so-called aggregates (see e.g. [68, 70]). The fine-level nodes are agglomerated and put into aggregates, which then represent “supernodes” on the next coarser level. The aggregation information together with the null space information of  $\mathbf{A}_0$  is used to construct the corresponding *tentative transfer operators*  $\widehat{\mathbf{R}}$  and  $\widehat{\mathbf{P}}$ . Transfer operators are necessary to transfer fine level information to the next coarser level (restriction) and from the coarse level to the next finer level (prolongation). For an efficient multigrid method, the transfer operators should transfer the low-frequency error modes, which are usually associated with large eigenvalues, to the coarse level, since they cannot be effectively reduced by iterative smoothing methods on the current level. On the coarsest level, a direct solver can take care of the remaining error modes. For smoothed aggregation multigrid (cf. [22, 68]), the prolongation operator is found by applying one smoothing sweep with a damped Jacobi iteration using

$$\mathbf{P} = \widehat{\mathbf{P}} - \omega \mathbf{D}^{-1} \mathbf{A} \widehat{\mathbf{P}} \quad (6)$$

with  $\mathbf{D}$  being the diagonal part of  $\mathbf{A}$  and a damping parameter  $\omega > 0$ . Depending on the symmetry of the system matrix  $\mathbf{A}$ , the restriction operator is either chosen as  $\mathbf{R} = \mathbf{P}^T$  or smoothed independently using, e.g. a Petrov-Galerkin approach (cf. [57]).

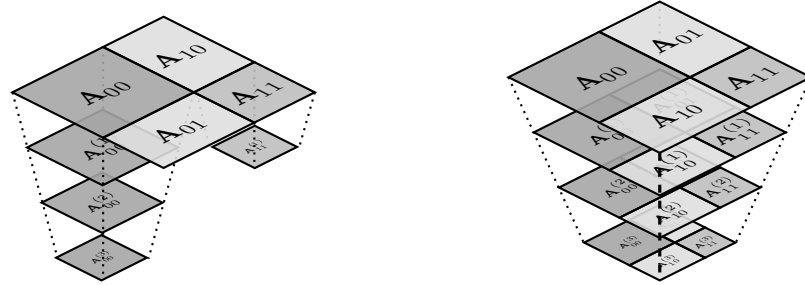
### 3.2. Algebraic multigrid methods for block matrices

Block matrices usually arise if multiple types of equations are coupled together. In the present context of contact problems in saddle point formulation, two types of equations, namely the balances of linear momentum of the solid bodies and the contact constraints, are connected via the off-diagonal blocks in (5). Similarly, multiphysics problems also yield block matrices where the coupling between different physical fields manifests itself in the off-diagonal blocks of the monolithic system matrix.

From a multigrid perspective, the most important question is where to consider the coupling between the different equations within the overall solver layout. In general, there are only two possible strategies to apply multigrid ideas to coupled block systems:

**Nested multigrid approach:** Multigrid methods can serve as local single field smoothers or solvers within well-known block preconditioners such as the SIMPLE method (cf. [44]) and variants for Schur complement based preconditioners or the block Gauss-Seidel (BGS) method. The coupling of the different fields or variables is only considered on the finest level in the outer (SIMPLE or BGS) iteration. This approach is well known in literature, e.g. for the Navier-Stokes equations [26, 61], fluid-structure interaction [23, 64] or general  $n$ -field problems [73]. The implementation is very easy and allows to use existing multigrid components in a standalone fashion within the solver. A graphic representation of this approach is shown in Figure 3a.

**Fully coupled multigrid approach:** Truly monolithic algebraic multigrid methods aim at coarsening the fully coupled fine level problem such that the block structure of the fine level matrix is preserved and the coupling information is present on all coarser levels, cf. Figure 3b. This is often achieved by using segregated transfer operators to preserve the characteristics of the sparsity pattern across all levels. Then, each level utilizes block smoothers to address the coupling. In [74], a coupled AMG method is developed and analyzed for a stabilized mixed finite element discretization of the Oseen equations. Fully coupled multigrid methods for multiphysics problems have been described in [23, 38, 73].



(a) Outer coupling iteration with nested multigrid methods. Example with four and nested coupling iteration on all multigrid levels for  $\mathbf{A}_{00}$  and  $\mathbf{A}_{11}$ . (b) Multiphysics multigrid approach with nested coupling iteration on all multigrid levels.

Figure 3. Multigrid for block matrices.

### 3.3. Designing algebraic multigrid methods for contact problems

In the present context, we can interpret the mortar contact problem in saddle point formulation as the coupling of two types of equations: the structural equations and the contact equations which serve as constraint equations. Since the contact constraint equations are only defined along the contact interface, we can further classify the mortar contact problem as an interface-coupled problem (in contrast to volume-coupled problems). This information is important for the choice of coarsening strategy. The contact constraint equations are also responsible for the characteristic saddle point structure, which needs special attention when choosing an appropriate coupling algorithm between the structural equations and the contact constraints. Considering the class of fully coupled AMG schemes, the generalized saddle point problem (5) has to be preserved on all multigrid levels such that the contact constraints are considered on all levels. Due to the constraints, this will require Schur complement based level smoothers on all levels.

Alltogether, the key ingredients for designing an algebraic multigrid method for contact problems in saddle point formulation are the coarsening strategy as proposed in Section 4 and the level smoother and the coupling iteration as detailed in Section 5.

## 4. A COARSENING STRATEGY FOR MORTAR CONTACT CONSTRAINTS

### 4.1. Segregated transfer operators

To keep the characteristic saddle point block structure (5) on all multigrid levels, the common approach is to use *segregated* transfer operators

$$\mathbf{P}_{\ell+1} = \begin{pmatrix} \mathbf{P}^u & 0 \\ 0 & \hat{\mathbf{P}}^\lambda \end{pmatrix}_{\ell+1} \quad \text{and} \quad \mathbf{R}_{\ell+1} = \begin{pmatrix} \mathbf{R}^u & 0 \\ 0 & \hat{\mathbf{R}}^\lambda \end{pmatrix}_{\ell+1}, \quad (7)$$

as, e.g. introduced in [7] or [1]. The segregated block transfer operators (7) are put together from the transfer operator blocks for the different physical and mathematical fields. Here,  $\mathbf{P}^u$  and  $\mathbf{R}^u$  describe the transfer operator blocks corresponding to the stiffness matrix block  $\mathbf{K}$  in (5). The transfer operators  $\hat{\mathbf{P}}^\lambda$  and  $\hat{\mathbf{R}}^\lambda$  define the level transfer for the Lagrange multipliers.

The block diagonal structure in (7) guarantees that the primary displacement variables and the secondary Lagrange multipliers are not “mixed up” on the coarser levels. That is, the coarse level matrix still has the same block structure with a clear distinction of momentum and constraint equations as for the fine level problem since the columns and rows of the transfer operators  $\mathbf{P}_{\ell+1}$  and  $\mathbf{R}_{\ell+1}$  can be interpreted as some kind of basis functions.

For many volume-coupled problems, for example in thermo-structure-interaction problems [15], it is straightforward to generate  $\hat{\mathbf{P}}^\lambda$  and  $\hat{\mathbf{R}}^\lambda$  to be consistent with  $\mathbf{P}^u$  and  $\mathbf{R}^u$ . That is, in context of smoothed aggregation algebraic multigrid we just use the same aggregates for building  $\mathbf{P}^u$  and  $\hat{\mathbf{P}}^\lambda$  (and the same for the restrictors, respectively).

For interface-coupled problems with interface constraints it is more difficult. Due to the saddle point structure of (5), the nonzero pattern of the  $\mathbf{Z}$  block is insufficient to generate valid aggregates for the Lagrange multipliers. Consequently, we need a special routine for finding aggregates for the Lagrange multipliers  $\lambda$  to be able to build the (non-smoothed) transfer operators  $\hat{\mathbf{P}}^\lambda$  and  $\hat{\mathbf{R}}^\lambda$ . Nevertheless it seems natural to reflect the aggregation information of the structural equations along the contact interface in the choice of the aggregates for the corresponding Lagrange multipliers  $\lambda$ .

### 4.2. Aggregation strategy for displacement variables

In order to preserve the physics of the fine level contact problem, it is important to keep the two solid bodies separated in the matrix representation on all coarse levels. Therefore, we apply the standard aggregation strategy to a modified  $\mathbf{K}$  block from (5), where all off-diagonal entries representing connections between the two solid bodies are dropped — in particular the matrix blocks  $\mathbf{K}_{\mathcal{I}\mathcal{M}}, \mathbf{K}_{\mathcal{A}\mathcal{M}}, \mathbf{K}_{\mathcal{M}\mathcal{I}}$  and  $\mathbf{K}_{\mathcal{M}\mathcal{A}}$  — in order to make sure that the resulting displacement aggregates  $\mathcal{A}_\ell^u$  do not cross the contact interface (see Figure 4). Neglecting these blocks during aggregation guarantees that the two solid bodies are not melted together in the coarse matrix representation. We stress that the modified  $\mathbf{K}$  is never formed explicitly, but rather the off-diagonal entries are dropped on the fly during the aggregation process.

### 4.3. Aggregation strategy for Lagrange multipliers

In contrast to geometric multigrid methods, there is not so much literature on aggregation-based AMG methods for contact problems in saddle point formulation. The only publication, the authors are aware of covering all aspects of smoothed aggregation methods for structural contact problems in saddle point formulation, is [1], which also discusses a special aggregation strategy for the Lagrange multipliers. To find aggregates  $\mathcal{A}_\ell^\lambda$  for the Lagrange multipliers, Adams [1] proposes to apply the standard aggregation algorithm to the graph of a suitable matrix representing the Lagrange multipliers. However, this approach has some drawbacks: First, the graph used for the aggregation of the Lagrange multipliers  $\lambda$  has to be built explicitly to serve as input for the standard aggregation algorithm. Secondly, one has to run the aggregation algorithm sequentially both for the displacement degrees of freedom and for the Lagrange multipliers. For the second run of the aggregation method, one might have to use a different set of aggregation parameters to obtain optimal results, which further increases the complexity for the user. Algorithmically, the resulting aggregates  $\mathcal{A}_\ell^\lambda$  for the Lagrange multipliers are built independently from the displacement aggregates  $\mathcal{A}_\ell^u$ .

In this work, we propose a different approach to build aggregates  $\mathcal{A}_\ell^\lambda$  for the Lagrange multipliers, which does not suffer from above drawbacks. Instead of explicitly building some helper matrix for the aggregation routine, interface aggregates  $\mathcal{A}_\ell^\lambda$  for the Lagrange multipliers are directly

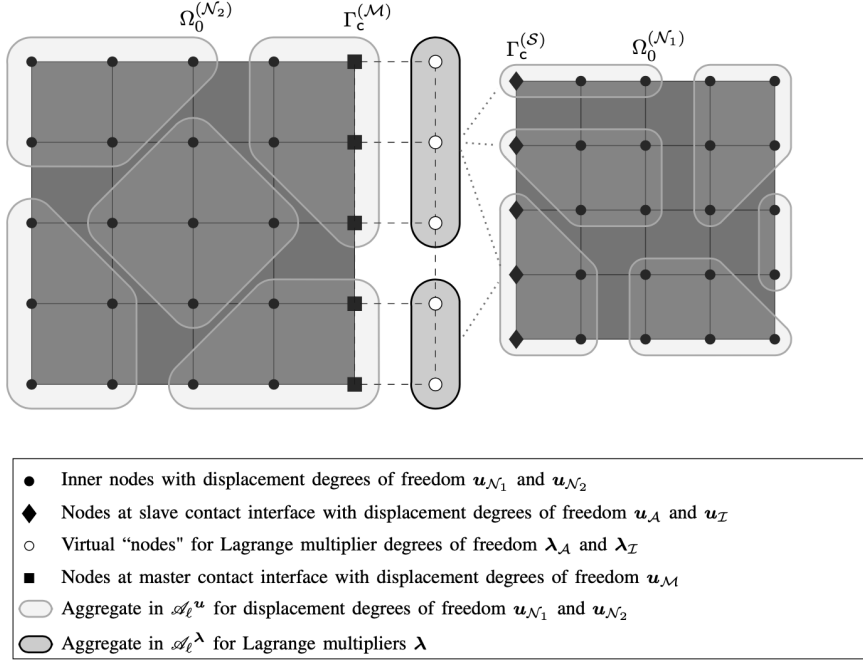


Figure 4. Aggregation for contact example in saddle point formulation.

generated using the aggregation information of the displacement variables (see Figure 4). The resulting interface aggregates for the Lagrange multipliers are by construction aligned with the corresponding displacement aggregates.

The exact aggregation procedure is described in Algorithm 1. Assuming that the standard aggregates  $\mathcal{A}_{\ell}^u$  for the displacement degrees of freedom are available, new aggregates  $\mathcal{A}_{\ell}^{\lambda}$  are built by collecting the corresponding Lagrange multiplier degrees of freedom. Beside the displacement aggregates  $\mathcal{A}_{\ell}^u$ , only the mortar matrix  $D$  is needed to algebraically reconstruct the contact interface and find the associated Lagrange multipliers. The new aggregates  $\mathcal{A}_{\ell}^{\lambda}$  for the Lagrange multipliers can be interpreted as the natural extension of the displacement aggregates  $\mathcal{A}_{\ell}^u$  at the interface. This facilitates to keep the ratio of coarse level nodes at the slave contact interface and the coarse Lagrange multipliers constant, which also balances the ratio of contact constraints and inner structural displacement degrees of freedom over all multigrid levels.

## 5. BLOCK SMOOTHING METHODS FOR MORTAR CONTACT PROBLEMS

Using saddle point preserving aggregation and segregated transfer operators as outlined in Section 4 to generate a fully coupled AMG hierarchy (see Section 3.3), block smoothing methods are the only algorithmic component which address the coupling of structural equilibrium equations and contact constraints on all levels of a fully coupled AMG hierarchy. Due to the saddle point problem resulting from the constraint-like contact equations, Schur complement based coupling iterations present themselves as ideal candidates to deal with the saddle point structure.

We now revisit some classical methods for saddle point systems, present them in a unified notation, and discuss and compare them in the context of contact problems.

### 5.1. Block smoothers for saddle point problems

Typical block smoothers consist of an outer coupling iteration with nested subsmothers or subsolvers to build (or approximate) the inverses of the diagonal blocks in the coupled block problem. Although all these methods are based on Schur complement approximations, there are different variants of block smoothers which can be interpreted as block extensions of classical iterative smoothing methods.

**Algorithm 1:** Aggregation algorithm for Lagrange multipliers.

---

**Procedure** `LagMultAggregation( $\mathcal{A}_\ell^u, D$ )`

    Initialize empty set and counter for aggregates  $\mathcal{A}_\ell^\lambda$   
 $\mathcal{A}_\ell^\lambda \leftarrow \emptyset, l \leftarrow 0$

    Initialize empty mapping of displacement aggregates to Lagrange multiplier aggregates  
 $d(k) \leftarrow \emptyset \quad \forall k = 1, \dots, m_{\mathcal{A}_\ell^u}$

    Loop over slave displacement DOFs (rows of D)  
**for**  $i \in \mathcal{D}_S$  **do**

        Find displacement node  $n^u$  id corresponding to displacement DOF  $i$   
 $n^u \leftarrow n(i)$

        Find aggregate index  $k$  that contains displacement node  $n^u$   
        Find  $k$  with  $\mathcal{A}_\ell^{(k)} \in \mathcal{A}_\ell^u$  where  $n^u \in \mathcal{A}_\ell^{(k)}$

        Loop over all Lagrange multipliers  $j$   
**for**  $j \in \mathcal{D}_\lambda$  **do**

            Check whether Lagrange multiplier  $j$  is coupled with row  $i$   
**if**  $D_{i,j} \neq 0$  **then**

                Find pseudo node  $n^\lambda$  for Lagrange multiplier  $j$   
 $n^\lambda \leftarrow n(j)$

                Check whether to build a new Lagrange multiplier aggregate  
**if**  $d(k) = \emptyset$  **then**

                    Increment internal aggregation counter  
 $l \leftarrow l + 1$

                    Build a new aggregate and add Lagrange multiplier node  $n^\lambda$   
 $\mathcal{A}_\ell^{(l)} \leftarrow \{n^\lambda\}$

                    Associate displacement aggregate  $k$  with Lagrange multiplier aggregate  $l$   
 $d(k) \leftarrow \{l\}$

                    Add new aggregate to set of Lagrange multiplier aggregates  $\mathcal{A}_\ell^\lambda$   
 $\mathcal{A}_\ell^\lambda \leftarrow \mathcal{A}_\ell^\lambda \cup \mathcal{A}_\ell^{(l)}$

**else**

                    Extend aggregate  $0 \leq d(k) \leq l$  with pseudo node  
 $\mathcal{A}_\ell^{(d(k))} \leftarrow \mathcal{A}_\ell^{(d(k))} \cup \{n^\lambda\}$

**end**

**end**

**end**

**end**

    Return aggregates for Lagrange multipliers  
**return**  $\mathcal{A}_\ell^\lambda$

---

The general block smoothing scheme can be written as

$$\begin{bmatrix} \Delta \mathbf{u}^{k+1} \\ \Delta \boldsymbol{\lambda}^{k+1} \end{bmatrix} = \begin{bmatrix} \Delta \mathbf{u}^k \\ \Delta \boldsymbol{\lambda}^k \end{bmatrix} + Q^{-1} \left( \begin{bmatrix} \mathbf{r}_u^k \\ \mathbf{r}_\lambda^k \end{bmatrix} - \begin{pmatrix} \mathbf{K} & \mathbf{C}_1^\top \\ \mathbf{C}_2 & -\mathbf{Z} \end{pmatrix} \begin{bmatrix} \Delta \mathbf{u}^k \\ \Delta \boldsymbol{\lambda}^k \end{bmatrix} \right) \quad (8)$$

where  $Q$  describes the  $2 \times 2$  block preconditioning matrix approximating the  $2 \times 2$  block operator in (5). In the following, a few classical block smoothers from literature (e.g. [43]) are introduced, stating that this list is by far not complete.

*5.1.1. Uzawa smoother* For the (inexact) Uzawa smoother, one chooses

$$Q := \frac{1}{\alpha} \begin{pmatrix} \mathbf{K} & 0 \\ \mathbf{C}_2 & -\tilde{S} \end{pmatrix}. \quad (9)$$

The parameter  $\alpha > 0$  is a damping parameter and  $\tilde{S}$  describes a cheap approximation of the Schur complement  $S$ . The better  $Q$  approximates the block operator from (5), the lower the number of linear iterations will be when using the block smoother within a multigrid preconditioner. For a theoretical review of Uzawa like smoothers, the reader is referred to [11, 19, 90].

With the off-diagonal coupling block  $C_2$  in (9), the smoother performs a one-way coupling in the sense that the Lagrange multiplier increments now depend on the current increment of the displacement degrees of freedom. In each smoothing iteration, one calculates a prediction for the displacement increments  $\delta\mathbf{u}^{k+1}$ , which are taken into account when solving for the corresponding Lagrange multiplier increments  $\delta\lambda^{k+1}$ .

---

**Algorithm 2:** Uzawa smoother.

---

**Procedure**  $\text{Uzawa}(\alpha, k_{\max})$

Apply  $k_{\max}$  smoothing sweeps with the Uzawa algorithm

**for**  $k \leftarrow 0$  **to**  $k_{\max} - 1$  **do**

*Prediction step: determine prediction increments  $\delta\mathbf{u}^{k+1}$  by solving approximately*  
 $\mathbf{K} \delta\mathbf{u}^{k+1} = \mathbf{r}_{\mathbf{u}}^k - \mathbf{K}\Delta\mathbf{u}^k - C_1^T \Delta\lambda^k$

*Correction step: Solve approximately for  $\delta\lambda^{k+1}$*   
 $-\tilde{S} \delta\lambda^{k+1} = \mathbf{r}_{\lambda}^k - C_2 \Delta\mathbf{u}^k + \mathbf{Z}\Delta\lambda^k - C_2 \delta\mathbf{u}^{k+1}$

*Update step: update solution variables*  
 $\Delta\mathbf{u}^{k+1} \leftarrow \Delta\mathbf{u}^k + \alpha \delta\mathbf{u}^{k+1}$   
 $\Delta\lambda^{k+1} \leftarrow \Delta\lambda^k + \alpha \delta\lambda^{k+1}$

**end**

*Return smooth solution vector*

**return**  $(\Delta\mathbf{u}^{k_{\max}}, \Delta\lambda^{k_{\max}})$

---

The error matrix for the Uzawa smoother is given by

$$\mathbf{E}_{\text{UZ}} := A - Q = \begin{pmatrix} \left(1 - \frac{1}{\alpha}\right)\mathbf{K} & C_1^T \\ \left(1 - \frac{1}{\alpha}\right)C_2 & -\mathbf{Z} + \frac{1}{\alpha}\tilde{S} \end{pmatrix}. \quad (10)$$

With  $\alpha = 1$  and  $\tilde{S} = \mathbf{Z} + C_2\tilde{\mathbf{K}}^{-1}C_1^T$  it is easy to verify that the error matrix of the Uzawa smoother reduces to

$$\mathbf{E}_{\text{UZ}} = \begin{pmatrix} 0 & C_1^T \\ 0 & C_2\tilde{\mathbf{K}}^{-1}C_1^T \end{pmatrix}. \quad (11)$$

That is, the Uzawa smoother cannot exactly fulfill the contact constraints in each iteration as the second block row in the error matrices (10) or (11) do not vanish.

*5.1.2. Braess–Sarazin smoother* Originally introduced for the Stokes problem by [7], the Braess–Sarazin smoother belongs to the class of block approximate smoothers and is based on the approximation

$$Q := \begin{pmatrix} \alpha\tilde{\mathbf{K}} & C_1^T \\ C_2 & -\mathbf{Z} \end{pmatrix} \approx \begin{pmatrix} \mathbf{K} & C_1^T \\ C_2 & -\mathbf{Z} \end{pmatrix} \quad (12)$$

of the block preconditioning matrix  $Q$  in (8). Here, the parameter  $\alpha > 0$  denotes a scaling parameter and  $\tilde{\mathbf{K}}$  describes an easy-to-invert approximation of  $\mathbf{K}$ . In practice, one uses the diagonal of  $\mathbf{K}$  as a cheap variant for the approximation  $\tilde{\mathbf{K}}$ , i.e.,  $\tilde{\mathbf{K}} = \text{diag}(\mathbf{K})$ .

The error matrix for the Braess–Sarazin smoother is calculated by

$$\mathbf{E}_{\text{BS}} := A - Q = \begin{pmatrix} \mathbf{K} - \alpha\tilde{\mathbf{K}} & 0 \\ 0 & 0 \end{pmatrix}. \quad (13)$$

The error matrix in (13) reveals that the second block row in the blocked operator (5) is correctly retained in (12). This makes the Braess–Sarazin smoother a reasonable choice for constrained problems such as structural contact problems. By splitting (12) into

$$\begin{pmatrix} \alpha\tilde{\mathbf{K}} & C_1^T \\ C_2 & -\mathbf{Z} \end{pmatrix} = \begin{pmatrix} \alpha\tilde{\mathbf{K}} & 0 \\ C_2 & -\mathbf{Z} - \frac{1}{\alpha}C_2\tilde{\mathbf{K}}^{-1}C_1^T \end{pmatrix} \begin{pmatrix} I & \frac{1}{\alpha}\tilde{\mathbf{K}}^{-1}C_1^T \\ 0 & I \end{pmatrix}, \quad (14)$$

**Algorithm 3:** Braess–Sarazin smoother.

---

**Procedure** BraessSarazin( $\alpha, k_{\max}$ )

*Apply  $k_{\max}$  smoothing sweeps with Braess–Sarazin algorithm*

**for**  $k \leftarrow 0$  **to**  $k_{\max} - 1$  **do**

*Prediction step: determine prediction  $\Delta\mathbf{u}^{k+\frac{1}{2}}$  by calculating*

$$\Delta\mathbf{u}^{k+\frac{1}{2}} = \Delta\mathbf{u}^k + \frac{1}{\alpha}\tilde{\mathbf{K}}^{-1}(\mathbf{r}_{\mathbf{u}}^k - \mathbf{K}\Delta\mathbf{u}^k - \mathbf{C}_1^T\Delta\boldsymbol{\lambda}^k)$$

*Correction step: Solve approximately for  $\Delta\boldsymbol{\lambda}^{k+\frac{1}{2}}$*

$$-(\mathbf{Z} + \frac{1}{\alpha}\mathbf{C}_2\tilde{\mathbf{K}}^{-1}\mathbf{C}_1^T)\Delta\boldsymbol{\lambda}^{k+\frac{1}{2}} = \mathbf{r}_{\boldsymbol{\lambda}}^k + \mathbf{Z}\Delta\boldsymbol{\lambda}^k - \mathbf{C}_2\Delta\mathbf{u}^{k+\frac{1}{2}}$$

*Update solution variables*

$$\Delta\boldsymbol{\lambda}^{k+1} \leftarrow \Delta\boldsymbol{\lambda}^k + \Delta\boldsymbol{\lambda}^{k+\frac{1}{2}}$$

$$\Delta\mathbf{u}^{k+1} \leftarrow \Delta\mathbf{u}^{k+\frac{1}{2}} - \frac{1}{\alpha}\tilde{\mathbf{K}}^{-1}\mathbf{C}_1^T\Delta\boldsymbol{\lambda}^{k+\frac{1}{2}}$$

**end**

*Return smooth solution vector*

**return**  $(\Delta\mathbf{u}^{k_{\max}}, \Delta\boldsymbol{\lambda}^{k_{\max}})$

---

the Braess–Sarazin algorithm can be defined as a prediction-correction scheme.

First, one solves for a prediction of the displacement variables  $\Delta\mathbf{u}^{k+\frac{1}{2}}$  and a tentative increment for the Lagrange multipliers  $\Delta\boldsymbol{\lambda}^{k+\frac{1}{2}} := \Delta\boldsymbol{\lambda}^{k+\frac{1}{2}} - \Delta\boldsymbol{\lambda}^k$  using

$$\begin{pmatrix} \alpha\tilde{\mathbf{K}} & 0 \\ \mathbf{C}_2 & -\mathbf{Z} - \frac{1}{\alpha}\mathbf{C}_2\tilde{\mathbf{K}}^{-1}\mathbf{C}_1^T \end{pmatrix} \begin{bmatrix} \Delta\mathbf{u}^{k+\frac{1}{2}} - \Delta\mathbf{u}^k \\ \Delta\boldsymbol{\lambda}^{k+\frac{1}{2}} - \Delta\boldsymbol{\lambda}^k \end{bmatrix} = \begin{bmatrix} \mathbf{r}_{\mathbf{u}}^k \\ \mathbf{r}_{\boldsymbol{\lambda}}^k \end{bmatrix} - \begin{pmatrix} \mathbf{K} & \mathbf{C}_1^T \\ \mathbf{C}_2 & -\mathbf{Z} \end{pmatrix} \begin{bmatrix} \Delta\mathbf{u}^k \\ \Delta\boldsymbol{\lambda}^k \end{bmatrix}. \quad (15)$$

Then, the corrected solution  $(\Delta\mathbf{u}^{k+1}, \Delta\boldsymbol{\lambda}^{k+1})$  is determined from

$$\begin{pmatrix} I & \frac{1}{\alpha}\tilde{\mathbf{K}}^{-1}\mathbf{C}_1^T \\ 0 & I \end{pmatrix} \begin{bmatrix} \Delta\mathbf{u}^{k+1} - \Delta\mathbf{u}^k \\ \Delta\boldsymbol{\lambda}^{k+1} - \Delta\boldsymbol{\lambda}^k \end{bmatrix} = \begin{bmatrix} \Delta\mathbf{u}^{k+\frac{1}{2}} - \Delta\mathbf{u}^k \\ \Delta\boldsymbol{\lambda}^{k+\frac{1}{2}} - \Delta\boldsymbol{\lambda}^k \end{bmatrix}. \quad (16)$$

As one can easily see from the Braess–Sarazin algorithm given in Algorithm 3, the prediction step can be understood as one hard-coded sweep with a (damped) Jacobi iteration. In other words, the quality of the prediction for the displacement degrees of freedom is rather poor, which is in contrast to the more accurate approximation of the contact constraints.

Note that the scaling parameter  $\alpha$  has a slightly different meaning than for other block smoothing methods such as the Uzawa smoother in Section 5.1.1. In the Braess–Sarazin method, it is used to weigh the different summands in the approximate Schur complement  $\mathbf{Z} + \frac{1}{\alpha}\mathbf{C}_2\tilde{\mathbf{K}}^{-1}\mathbf{C}_1^T$  relatively to each other.

**5.1.3. SIMPLE variants** Originally introduced in [44], the SIMPLE method is based on the approximate block factorization

$$Q := \begin{pmatrix} \mathbf{K} & 0 \\ \mathbf{C}_2 & -\tilde{S} \end{pmatrix} \begin{pmatrix} I & \tilde{\mathbf{K}}^{-1}\mathbf{C}_1^T \\ 0 & \frac{1}{\alpha}I \end{pmatrix} = \begin{pmatrix} \mathbf{K} & \mathbf{K}\tilde{\mathbf{K}}^{-1}\mathbf{C}_1^T \\ \mathbf{C}_2 & \left(1 - \frac{1}{\alpha}\right)\mathbf{C}_2\tilde{\mathbf{K}}^{-1}\mathbf{C}_1^T - \frac{1}{\alpha}\mathbf{Z} \end{pmatrix} \approx \begin{pmatrix} \mathbf{K} & \mathbf{C}_1^T \\ \mathbf{C}_2 & -\mathbf{Z} \end{pmatrix} \quad (17)$$

for (8). In (17),  $\tilde{S}$  denotes an approximation of the Schur complement  $S := \mathbf{Z} + \mathbf{C}_2\mathbf{K}^{-1}\mathbf{C}_1^T$  with a cheap and easy-to-invert approximation  $\tilde{\mathbf{K}}$  of the block  $\mathbf{K}$ . Equation (8) with  $Q$  from (17) can be reformulated as

$$\begin{pmatrix} \mathbf{K} & 0 \\ \mathbf{C}_2 & -\tilde{S} \end{pmatrix} \begin{pmatrix} I & \tilde{\mathbf{K}}^{-1}\mathbf{C}_1^T \\ 0 & \frac{1}{\alpha}I \end{pmatrix} \begin{bmatrix} \Delta\mathbf{u}^{k+1} - \Delta\mathbf{u}^k \\ \Delta\boldsymbol{\lambda}^{k+1} - \Delta\boldsymbol{\lambda}^k \end{bmatrix} = \begin{bmatrix} \mathbf{r}_{\mathbf{u}}^k \\ \mathbf{r}_{\boldsymbol{\lambda}}^k \end{bmatrix} - \begin{pmatrix} \mathbf{K} & \mathbf{C}_1^T \\ \mathbf{C}_2 & \mathbf{Z} \end{pmatrix} \begin{bmatrix} \Delta\mathbf{u}^k \\ \Delta\boldsymbol{\lambda}^k \end{bmatrix}, \quad (18)$$

which leads to a two step predictor-corrector scheme, i.e., first solve

$$\begin{pmatrix} \mathbf{K} & 0 \\ \mathbf{C}_2 & -\tilde{S} \end{pmatrix} \begin{bmatrix} \Delta\mathbf{u}^{k+\frac{1}{2}} - \Delta\mathbf{u}^k \\ \Delta\boldsymbol{\lambda}^{k+\frac{1}{2}} - \Delta\boldsymbol{\lambda}^k \end{bmatrix} = \begin{bmatrix} \mathbf{r}_{\mathbf{u}}^k \\ \mathbf{r}_{\boldsymbol{\lambda}}^k \end{bmatrix} - \begin{pmatrix} \mathbf{K} & \mathbf{C}_1^T \\ \mathbf{C}_2 & \mathbf{Z} \end{pmatrix} \begin{bmatrix} \Delta\mathbf{u}^k \\ \Delta\boldsymbol{\lambda}^k \end{bmatrix} \quad (19)$$

for an intermediate solution of the displacement variable  $\Delta\mathbf{u}^{k+\frac{1}{2}}$  with a subsequent adaption of the Lagrange multipliers  $\Delta\lambda^{k+\frac{1}{2}}$  and then obtain the final solution by

$$\begin{pmatrix} I & \tilde{\mathbf{K}}^{-1}\mathbf{C}_1^T \\ 0 & \frac{1}{\alpha}I \end{pmatrix} \begin{bmatrix} \Delta\mathbf{u}^{k+1} - \Delta\mathbf{u}^k \\ \Delta\lambda^{k+1} - \Delta\lambda^k \end{bmatrix} = \begin{bmatrix} \Delta\mathbf{u}^{k+\frac{1}{2}} - \Delta\mathbf{u}^k \\ \Delta\lambda^{k+\frac{1}{2}} - \Delta\lambda^k \end{bmatrix}. \quad (20)$$

The full SIMPLE method is given in Algorithm 4.

---

**Algorithm 4:** SIMPLE smoother.

---

**Procedure** SIMPLE( $\alpha, k_{\max}$ )

*Apply  $k_{\max}$  smoothing sweeps with SIMPLE algorithm*  
**for**  $k \leftarrow 0$  **to**  $k_{\max} - 1$  **do**  
  *Prediction step: determine prediction  $\Delta\mathbf{u}^{k+\frac{1}{2}}$  by solving approximately*  
   $\mathbf{K}\Delta\mathbf{u}^{k+\frac{1}{2}} = \mathbf{r}_{\mathbf{u}}^k - \mathbf{C}_1^T\Delta\lambda^k$   
  *Correction step: Solve approximately for  $\delta\lambda^{k+\frac{1}{2}}$*   
   $-\tilde{\mathbf{S}}\delta\lambda^{k+\frac{1}{2}} = \mathbf{r}_{\lambda}^k + \mathbf{Z}\Delta\lambda^k - \mathbf{C}_2\Delta\mathbf{u}^{k+\frac{1}{2}}$   
  *Update step: update solution variables*  
   $\Delta\lambda^{k+1} \leftarrow \Delta\lambda^k + \alpha\delta\lambda^{k+\frac{1}{2}}$   
   $\Delta\mathbf{u}^{k+1} \leftarrow \Delta\mathbf{u}^{k+\frac{1}{2}} - \alpha\tilde{\mathbf{K}}^{-1}\mathbf{C}_1^T\delta\lambda^{k+\frac{1}{2}}$   
**end**  
*Return smooth solution vector*  
**return**  $(\Delta\mathbf{u}^{k_{\max}}, \Delta\lambda^{k_{\max}})$

---

The error for one sweep with the SIMPLE method is calculated as

$$\mathbf{E}_{\text{SIMPLE}} := \mathbf{A} - \mathbf{Q} = \begin{pmatrix} 0 & \mathbf{C}_1^T - \mathbf{K}\tilde{\mathbf{K}}^{-1}\mathbf{C}_1^T \\ 0 & -\mathbf{Z} - \mathbf{C}_2\tilde{\mathbf{K}}^{-1}\mathbf{C}_1^T + \frac{1}{\alpha}\tilde{\mathbf{S}} \end{pmatrix}. \quad (21)$$

As one can see from (21), SIMPLE does not affect the terms that operate on the primary displacement variables, but it perturbs the Lagrange multipliers. Choosing  $\tilde{\mathbf{S}} = \alpha\mathbf{Z} + \alpha\mathbf{C}_2\tilde{\mathbf{K}}^{-1}\mathbf{C}_1^T$ , the error matrix reduces to

$$\mathbf{E}_{\text{SIMPLE}} = \begin{pmatrix} 0 & \mathbf{C}_1^T - \mathbf{K}\tilde{\mathbf{K}}^{-1}\mathbf{C}_1^T \\ 0 & 0 \end{pmatrix}. \quad (22)$$

That is, an appropriate approximation  $\tilde{\mathbf{S}}$  of the Schur complement  $\mathbf{S}$  allows to exactly satisfy the contact constraints within one smoothing sweep.

The concrete choice for the approximation  $\tilde{\mathbf{K}}$  of the block  $\mathbf{K}$  and the approximation  $\tilde{\mathbf{S}}$  for the Schur complement operator gives rise to different variants of the SIMPLE method. Now, we only list those variants that are used later in the numerical examples in Section 6.

**SIMPLE:** The classical SIMPLE method (cf. [44, 45]) uses  $\tilde{\mathbf{K}} = \text{diag}(\mathbf{K})$  as easy-to-invert approximation  $\tilde{\mathbf{K}}$  of  $\mathbf{K}$ , together with  $\tilde{\mathbf{S}} = \mathbf{Z} + \mathbf{C}_2(\text{diag}(\mathbf{K}))^{-1}\mathbf{C}_1^T$ . The damping parameter  $\alpha$  is chosen from the interval  $(0, 1]$  and damps the update for the Lagrange multipliers (cf. [18]).

**SIMPLEC:** Variants of the SIMPLE method like SIMPLEC as introduced in [67] can be understood as an enhancement of the classical SIMPLE method. The general idea is to provide better approximations for the inverse of the block  $\mathbf{K}$ . Instead of just using the diagonal of  $\mathbf{K}$  for calculating the approximate inverse of  $\mathbf{K}$ , the diagonal matrix containing the row sums of  $|\mathbf{K}| = (|a_{ij}|)_{i,j=1,\dots,n_K}$  is used. That is,  $\tilde{\mathbf{K}}$  is defined as

$$\tilde{\mathbf{K}} = \text{diag}\left(\sum_{j=1}^{n_K} |a_{ij}|\right), \quad i = 1, \dots, n_K. \quad (23)$$

The default choice for  $\tilde{\mathbf{S}}$  is consequently  $\tilde{\mathbf{S}} = \alpha\mathbf{Z} + \alpha\mathbf{C}_2\tilde{\mathbf{K}}^{-1}\mathbf{C}_1^T$  with  $\tilde{\mathbf{K}}$  as defined in (23). So, the method is very similar to the classical SIMPLE method (cf. [18]).

### 5.2. Comparison of saddle point smoothing methods

**5.2.1. Cheap variants of block smoothers** Based on the block splitting from (5), all block smoothing methods from Section 5.1 internally have to build the inverses of the matrix blocks on the diagonal. To keep the computational costs low, one does not solve for the block inverses exactly, but only applies a fixed number of smoothing sweeps with a relaxation-based method. The numerical examples in Section 6 show that such an approximation leads to efficient block smoothing methods. As a naming convention, the prefix "Cheap" is added to the name of the block smoothing method to indicate the usage of a cheap approximation for finding the inverse of the diagonal blocks. A more theoretical discussion on the mathematical consequences of approximations for the Schur complement  $S$  can be found in [89].

**5.2.2. Block smoothers for contact problems** The coupling of the different solid blocks at the contact interface is at the core of any contact problem. Mathematically, the contact problem is governed by the contact constraint equations. Since the coupling of the structural blocks takes place in the level smoother only, constraint smoothers (cf. [35]) are preferred, which put some special focus on the consideration of the constraint equations. In our case, the preferred choices are the block approximate smoothers such as the Braess–Sarazin and SIMPLE-based methods from Sections 5.1.2 and 5.1.3, respectively, as they represent the contact constraints exactly. As seen from (11), an Uzawa smoother cannot satisfy the contact constraints exactly and, thus, is excluded from further considerations.

In the Braess–Sarazin method, the approximation  $\tilde{K} = \text{diag}(K)$  is hard-coded with some scaling parameter  $\alpha > 0$  and consistently used within the approximate Schur complement operator, which is defined by  $\tilde{S} = Z + \frac{1}{\alpha} C_2 \tilde{K}^{-1} C_1^\top$ . The scaling parameter  $\alpha$  weights the different summands in the Schur complement operator  $\tilde{S}$ , whereas in the SIMPLE algorithm the  $\alpha$  can be understood as a pure damping parameter.

In contrary to the Braess–Sarazin method, the SIMPLE based methods keep the full  $K$  block whenever possible in the block factorization and use  $\tilde{K}$  only where its inverse is required. Consequently, in "cheap" variants of the SIMPLE method, more elaborate smoothing strategies can be used for the  $K$  block instead of a hard-coded Jacobi sweep. Therefore, one can think of the SIMPLE methods to allow for a more balanced quality of approximations for the displacement degrees of freedom and Lagrange multipliers for the contact constraints, whereas the Braess–Sarazin method exhibits an imbalance in the sense that the computational effort spent for approximating the constraints is much higher than for dealing with the displacement variables.

When using exact arithmetic, comparing the error matrices of the Braess–Sarazin smoother and the SIMPLE smoother shows that the Braess–Sarazin smoother preserves the contact constraints per default due to the fixed definition of the Schur complement operator. A similar behavior for the SIMPLE smoother can only be found when using a properly scaled approximation of the Schur complement (see the discussion of (22)).

## 6. NUMERICAL EXAMPLES

For the numerical examples, we use our in-house code BACI, that internally uses various capabilities from the Trilinos project<sup>†</sup>. The implementation of the multigrid algorithms is based on Trilinos' MueLu package [4, 77]. In particular, all block smoothers from Section 5 are readily available in MueLu. The contact specific aggregation for the Lagrange multiplier unknowns from Section 4 is implemented in the MueLu framework, however not publicly available, yet.

### 6.1. Two solid bodies example

Motivated by findings in our previous work [78], this example briefly revisits a detail that has been problematic in the context of contact problems in condensed formulations. While the discrete global unknowns  $(\mathbf{u}, \boldsymbol{\lambda})$  are – as usual – formulated with respect to the global Cartesian frame, the discrete Lagrange multiplier weights  $\boldsymbol{\mu}$  and therefore the contact constraint equations in (3b) and (3c) are formulated with respect to a local convective coordinate system. This local system is defined at each slave node  $j$  by a surface normal vector and two tangent vectors, i.e. by a triad of orthonormal basis vectors  $(\mathbf{n})_j$ ,  $(\boldsymbol{\tau}_\xi)_j$  and  $(\boldsymbol{\tau}_\eta)_j$ . Although it represents a quite intuitive and natural choice in contact mechanics, this local constraint formulation may lead to non-diagonally dominant system matrices

<sup>†</sup><https://trilinos.github.io>

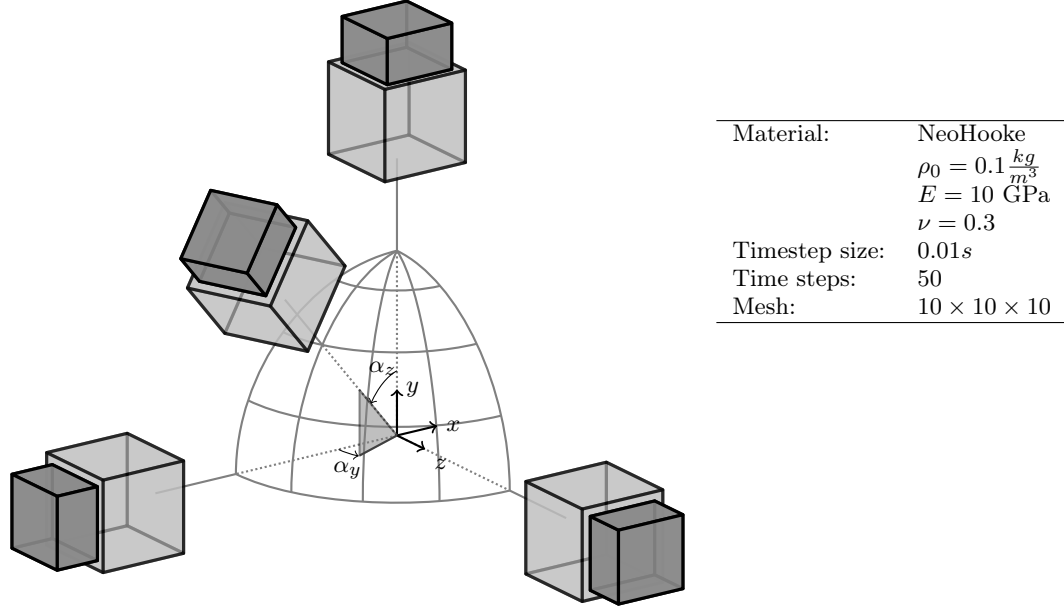


Figure 5. Two solid bodies example – Geometric configuration and model parameters for two solid bodies example.

and therefore poses a serious challenge to the development of iterative linear solvers as has been elaborated in [78]. In the following, we will investigate the susceptibility of the proposed saddle point preconditioners to this phenomenon.

**6.1.1. Setup** A simple 3D contact example is used as shown in Figure 5. Looking exemplarily at the case  $\alpha_y = \alpha_z = 0$ , one has two solid bodies with the same material parameters using a Neo-Hookean material ( $\rho_0 = 0.1 \frac{kg}{m^3}$ ,  $E = 10$  GPa,  $\nu = 0.3$ ). The initial gap between the two solid bodies is 0.02 units. The upper solid body (size:  $0.8 \times 0.8 \times 0.5$  units) is moving down with constant velocity along the normal to the contact interface towards the lower fixed solid body (size:  $1.0 \times 1.0 \times 1.0$  units). If not stated otherwise, a  $10 \times 10 \times 10$  mesh is used for the discretization of each solid body. The simulation runs for 40 time steps with a time step size of 0.01s on 4 processors. After 6 time steps ( $t = 0.06s$ ) both bodies come into contact and are deformed. We assume frictionless contact here. The idea is to reduce contact-specific effects (contact search for active set of nodes) to a minimum, such that one can focus on the linear solvers. That is, the contact zone is not changing once the two solid bodies are in contact.

Of course, one expects the behavior of the linear solver to be independent of the exact geometric configuration. In particular, the number of linear iterations should be independent of the rotation angles  $\alpha_y$  and  $\alpha_z$ , since the underlying physics do not change. For reasons of symmetry, it is sufficient to vary  $\alpha_y$  and  $\alpha_z$  within  $0 \leq \alpha_y, \alpha_z \leq \frac{\pi}{2}$ .

The spatial discretization is based on a  $10 \times 10 \times 10$  mesh for each solid block with altogether 6000 displacement degrees of freedom and 300 Lagrange multipliers modeling the contact coupling constraints for the  $10 \times 10$  slave nodes at the contact interface.

**6.1.2. Stopping criteria** The nonlinear iteration inside each time step stops if either  $\|\Delta \mathbf{u}\|_e < 10^{-8}$  holds for the Newton increment of the displacement degrees of freedom, or alternatively, if the conditions

$$\|\mathbf{r}_i^u\|_e < 10^{-6} \wedge \|\mathbf{r}_i^\lambda\|_e < 10^{-4} \quad (24)$$

hold for the nonlinear residuals  $\mathbf{r}_i^u$  and  $\mathbf{r}_i^\lambda$  in (4) after applying  $i$  Newton iterations. Thereby,  $\|\bullet\|_e$  denotes the Euclidian vector norm. Within each Newton iteration, the saddle point system (4) is solved iteratively using a preconditioned GMRES method with a 3-level AMG preconditioner as described

in Section 3. The iterative process for the linear system is considered to be converged, if it is

$$\left\| \frac{\mathbf{r}^k}{\mathbf{r}^0} \right\|_e < 10^{-8} \quad (25)$$

for the full residual vector  $\mathbf{r}^k = \begin{bmatrix} \mathbf{r}^u \\ \mathbf{r}^\lambda \end{bmatrix}$  in the linear iteration step  $k$ . Here, the subscript  $i$  for the nonlinear Newton iteration is dropped.

In this work, we focus on the behavior of the linear solver. Therefore, a fixed stopping criterion is chosen in (25). This allows the comparison of different preconditioning techniques including their effect on the linear solution strategy. For real world problems, and especially for coupled multiphysics problems, the task of choosing appropriate stopping criteria for both the nonlinear and linear solver turns out to be quite challenging. Usually, one would choose a combination of different (length-scaled) norms for the partial vectors. In order to reduce the solver time in the inner linear solver, it is recommended to adapt the linear (relative) solver tolerance according to the residual norms of the outer nonlinear solver.

**6.1.3. Results** First, the effect of the different saddle point smoothers on the number of linear iterations is explored. Table I summarizes the average number of linear iterations per time step for different combinations of the rotation angles  $\alpha_y$  and  $\alpha_z$ . The numbers in brackets denote the maximum number of linear iterations needed for solving one linear system during the full simulation, roughly indicating the variation of the number of linear iterations within the simulation. For the CheapUzawa smoother, the number of iterations does not show a dependence on the rotation angles  $\alpha_y$  and  $\alpha_z$ . Comparing the numbers from Table Ia with the results for the CheapBraessSarazin smoother in Table Ib, the CheapBraessSarazin smoother heavily suffers from the worse approximation of the displacement degrees of freedom using one internal hard-coded Jacobi sweep (cf. Section 5.1.2). The resulting iteration numbers show an obvious dependency on the rotation angles. With a CheapSIMPLEC block smoother, the number of iterations is lower than for the CheapUzawa smoother and independent from  $\alpha_y$  and  $\alpha_z$  when compared with the CheapBraessSarazin smoother (see Table Ic). So, the linear solver has some benefit from the two-way coupling of displacements and Lagrange multipliers within the AMG preconditioner. Compared to the Uzawa smoother, the additional computational costs are very low with only one additional matrix-vector product by  $\tilde{\mathbf{K}}^{-1} \mathbf{C}_1^T$  per iteration. Therefore, CheapSIMPLEC is the preferred level smoother for our further experiments with some cheap approximations for the internal single fields using some sweeps with a (symmetric) Gauss–Seidel (SGS) method or incomplete LU factorization (ILU).

Table II illustrates how the number of CheapSIMPLEC coupling iterations and the quality of the single field smoothing methods within the CheapSIMPLEC smoother affect the number of linear iterations. Improving the quality of the Schur complement approximations within CheapSIMPLEC (see Tables IIa vs. IIb) as well as increasing the number of CheapSIMPLEC coupling iterations (see Table IIc) unsurprisingly reduces the number of linear solver iterations. Aside from the concrete parameter choices for the level smoother, one can even further reduce the number of linear iterations with a reasonable transfer operator smoothing strategy for the displacement block, e.g. as indicated in (6).

By intention there are no solver timings given as the example is too small to perform reasonable measurements, especially when using 4 processors for altogether only 6300 degrees of freedom.

The intention of this example is to compare typical saddle point smoothers within a fully coupled AMG preconditioner. One can observe the expected behavior that increasing the number of smoothing sweeps reduces the number of linear GMRES iterations. However, in practice, the variant with a smaller number of GMRES iterations may not always be the fastest method. This example shows that the proper choice of block level smoothing is essential for the overall performance of a saddle point multigrid method. The particular choice of the block smoothing method gives the user full control over the quality of the coupling with field-specific parameters and allows for fine-grained adaptions and problem-specific optimizations.

With the experience from this example one can choose efficient level smoothers which provide results independent from the exact geometric configuration. In the next examples, we will put attention on effects for the linear solver caused by changes in the active set of contact nodes for larger problems.

## 6.2. 1000 deformable rings

**6.2.1. Setup** This example consists of 1000 deformable rings (Neo-Hookean material with  $E = 210$ ,  $\nu = 0.3$  and  $\rho_0 = 7.83 \cdot 10^{-6}$ ) arranged in a rectangle (see Figure 6). A gravitational force is inducing

Table I. Two solid bodies example – Average (maximum) number of linear GMRES iterations per nonlinear iteration (over all 40 time steps) for different combinations of rotation angles  $\alpha_y$  and  $\alpha_z$ . As preconditioner, a 3 level AMG method (PA-AMG + PA-AMG, minimum aggregate size: 6 nodes) is used with different level smoothers.

(a) **Level smoother:** 3 CheapUzawa(0.7) with 1 SGS (0.7) + ILU(0)

		$\alpha_y$					
		0	$\frac{1}{8}\pi$	$\frac{1}{4}\pi$	$\frac{3}{8}\pi$	$\frac{1}{2}\pi$	
		0	26.2 (30)	26.0 (30)	24.6 (29)	24.6 (30)	26.0 (29)
		$\frac{1}{8}\pi$	26.8 (30)	25.8 (37)	25.3 (30)	24.7 (30)	27.3 (31)
		$\frac{1}{4}\pi$	25.9 (31)	25.1 (32)	25.3 (30)	28.7 (40)	26.0 (31)
		$\frac{3}{8}\pi$	25.9 (31)	25.0 (30)	24.9 (30)	25.5 (33)	25.3 (29)
		$\frac{1}{2}\pi$	26.1 (30)	25.4 (32)	25.5 (30)	26.8 (31)	26.0 (30)

(b) **Level smoother:** 3 CheapBraessSarazin(1.9) with ILU(0))

		$\alpha_y$					
		0	$\frac{1}{8}\pi$	$\frac{1}{4}\pi$	$\frac{3}{8}\pi$	$\frac{1}{2}\pi$	
		0	29.9 (37)	29.6 (36)	27.9 (33)	30.7 (38)	29.7 (37)
		$\frac{1}{8}\pi$	41.2 (59)	43.1 (68)	42.0 (58)	43.6 (63)	41.4 (59)
		$\frac{1}{4}\pi$	56.8 (82)	64.8 (86)	68.6 (95)	64.3 (86)	54.9 (75)
		$\frac{3}{8}\pi$	40.9 (60)	55.5 (74)	73.1 (102)	111.1 (141)	41.3 (61)
		$\frac{1}{2}\pi$	29.9 (37)	41.0 (55)	56.8 (79)	41.3 (61)	29.7 (36)

(c) **Level smoother:** 3 CheapSIMPLEC(0.5) with 1 SGS (0.7) + ILU(0)

		$\alpha_y$					
		0	$\frac{1}{8}\pi$	$\frac{1}{4}\pi$	$\frac{3}{8}\pi$	$\frac{1}{2}\pi$	
		0	20.5 (26)	19.3 (21)	18.8 (23)	19.3 (26)	19.3 (20)
		$\frac{1}{8}\pi$	20.1 (22)	19.7 (27)	20.0 (24)	19.8 (21)	21.2 (25)
		$\frac{1}{4}\pi$	20.1 (25)	19.9 (23)	20.1 (23)	22.0 (26)	20.8 (30)
		$\frac{3}{8}\pi$	19.7 (22)	19.8 (22)	19.8 (23)	20.0 (26)	19.7 (23)
		$\frac{1}{2}\pi$	19.3 (20)	19.6 (22)	20.4 (27)	20.7 (25)	20.5 (28)

an acceleration towards a rigid wall. The simulated time extends to 2.0s with a time step size of  $\Delta t = 0.0005s$ , yielding 4000 time steps in total. The full mesh consists 110000 nodes with 110 nodes for each deformable ring.

*6.2.2. Stopping criteria* In each time step, the nonlinear system is handled by a semi-smooth Newton method. As convergence criteria, we have chosen

$$\|\Delta \mathbf{u}\|_e < 10^{-8} \wedge \left( \|\mathbf{r}_i^u\|_e < 10^{-8} \wedge \left\| \mathbf{r}_i^\lambda \right\|_e < 10^{-6} \right). \quad (26)$$

Here,  $\mathbf{r}_i^u$  and  $\mathbf{r}_i^\lambda$  denote the nonlinear residual for the displacement and Lagrange multiplier variables after  $i$  Newton iterations, respectively. Similarly,  $\Delta \mathbf{u}$  denotes the solution increment for the displacement variables in the  $i$ -th Newton iteration.

Table II. Two solid bodies example – Average (maximum) number of linear GMRES iterations per nonlinear iteration (over all 40 time steps) for different rotation angles  $\alpha_y$  and  $\alpha_z$ . As preconditioner, a 3 level AMG method (minimum aggregate size: 6 nodes) is used with different variants of CheapSIMPLEC.

(a) **Level smoother:** 1 CheapSIMPLEC(0.7) with 1 SGS (0.7) + ILU(0)

		$\alpha_y$				
		0	$\frac{1}{8}\pi$	$\frac{1}{4}\pi$	$\frac{3}{8}\pi$	$\frac{1}{2}\pi$
$\tilde{\alpha}_z$	0	37.5 (57)	35.6 (43)	35.2 (46)	36.1 (44)	35.7 (45)
	$\frac{1}{8}\pi$	36.4 (45)	37.6 (44)	38.5 (47)	36.3 (43)	38.1 (53)
	$\frac{1}{4}\pi$	39.1 (50)	37.8 (47)	37.0 (47)	39.2 (48)	37.0 (44)
	$\frac{3}{8}\pi$	36.3 (43)	37.0 (48)	37.8 (46)	37.2 (51)	36.4 (43)
	$\frac{1}{2}\pi$	36.2 (47)	38.0 (51)	39.8 (50)	36.9 (50)	36.6 (53)

(b) **Level smoother:** 1 CheapSIMPLEC(0.7) with 3 SGS (0.7) + ILU(0)

		$\alpha_y$				
		0	$\frac{1}{8}\pi$	$\frac{1}{4}\pi$	$\frac{3}{8}\pi$	$\frac{1}{2}\pi$
$\tilde{\alpha}_z$	0	29.5 (41)	27.5 (34)	28.4 (36)	28.5 (37)	27.1 (36)
	$\frac{1}{8}\pi$	29.3 (37)	30.1 (40)	32.7 (40)	28.8 (35)	28.4 (38)
	$\frac{1}{4}\pi$	30.0 (35)	29.6 (37)	28.5 (37)	31.1 (38)	29.2 (36)
	$\frac{3}{8}\pi$	28.8 (36)	27.8 (34)	28.1 (34)	29.1 (39)	28.1 (34)
	$\frac{1}{2}\pi$	28.5 (38)	28.4 (34)	29.7 (40)	27.9 (35)	27.1 (35)

(c) **Level smoother:** 3 CheapSIMPLEC(0.7) with 3 SGS (0.7) + ILU(0)

		$\alpha_y$				
		0	$\frac{1}{8}\pi$	$\frac{1}{4}\pi$	$\frac{3}{8}\pi$	$\frac{1}{2}\pi$
$\tilde{\alpha}_z$	0	15.5 (16)	17.0 (19)	16.9 (20)	15.3 (16)	15.2 (16)
	$\frac{1}{8}\pi$	16.2 (17)	16.1 (17)	16.3 (17)	15.9 (17)	16.1 (17)
	$\frac{1}{4}\pi$	16.0 (17)	16.0 (17)	16.0 (17)	15.6 (18)	15.6 (16)
	$\frac{3}{8}\pi$	15.7 (17)	15.9 (17)	15.9 (17)	15.5 (19)	15.6 (16)
	$\frac{1}{2}\pi$	15.6 (16)	15.8 (16)	15.7 (16)	15.4 (16)	15.1 (16)

Due to the saddle point formulation, the effective size of the linear system is changing with the number of active contact nodes. Since the underlying contact configurations are changing drastically, it turns out to be a good example for testing the robustness of the preconditioners. A GMRES solver is applied for the linear systems with different variants of AMG preconditioners. The relative tolerance of convergence for the GMRES solver is set to  $\left\| \frac{\mathbf{r}^k}{\mathbf{r}^0} \right\|_e < 10^{-8}$  with  $\mathbf{r}^k = \begin{bmatrix} \mathbf{r}^{\mathbf{u}} \\ \mathbf{r}^{\boldsymbol{\lambda}} \end{bmatrix}$  being the full residual vector in the linear iteration step  $k$ . Again, the subscript  $i$  for the nonlinear Newton step is dropped.

**6.2.3. Results** Table III provides an overview of the chosen preconditioner parameters for the level smoothers. For each class of multigrid preconditioners, only those variants are presented, that give the best overall timings and are able to accomplish the all 4000 time steps of the full simulation.

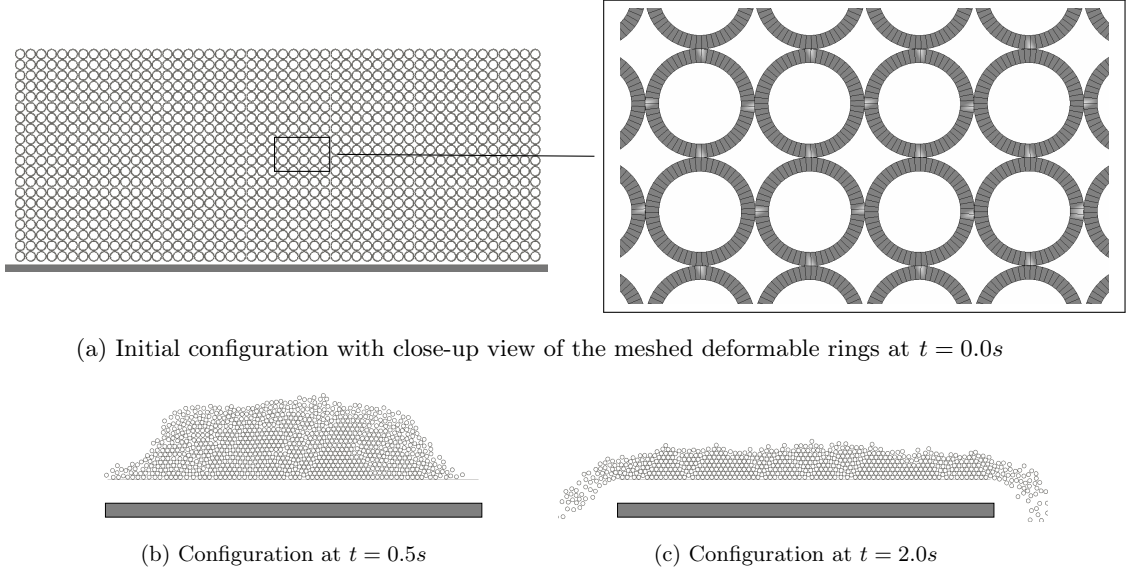


Figure 6. 1000 deformable rings – Characteristic stages at different times.

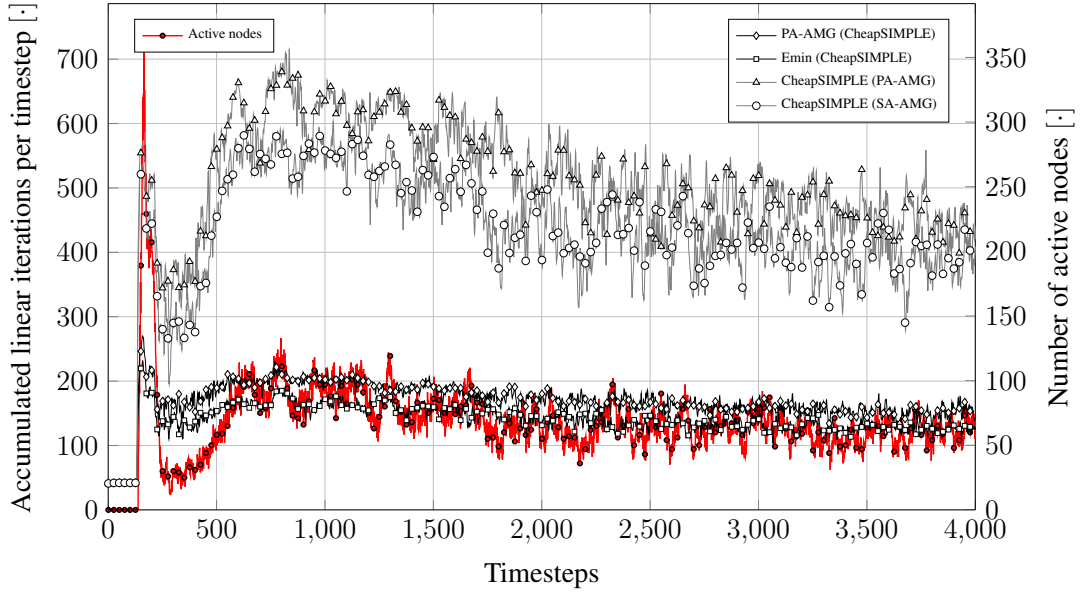
Table III. 1000 deformable rings – Different AMG variants.

Preconditioner type	
Full multigrid based methods	Nested multigrid based methods
<b>PA-AMG (CheapSIMPLE)</b> Transfer operators: PA-AMG Level smoother: 1 CheapSIMPLEC(0.8) – Pred. smoother: 3 SGS (0.8) – Corr. smoother: ILU (0)	<b>CheapSIMPLE (PA-AMG)</b> Block prec.: 1 CheapSIMPLEC(0.8) – Pred. smoother: AMG – Transfer op.: PA-AMG – Level sm.: 1 SGS (0.8) – Corr. smoother: KLU
<b>Emin (CheapSIMPLE)</b> Transfer operators: Emin Level smoother: 1 CheapSIMPLEC(0.8) – Pred. smoother: 3 SGS (0.8) – Corr. smoother: ILU (0)	<b>CheapSIMPLE (SA-AMG)</b> Block prec.: 1 CheapSIMPLEC(0.8) – Pred. smoother: AMG – Transfer op.: SA-AMG (0.8) – Level sm.: 1 SGS (0.8) – Corr. smoother: KLU

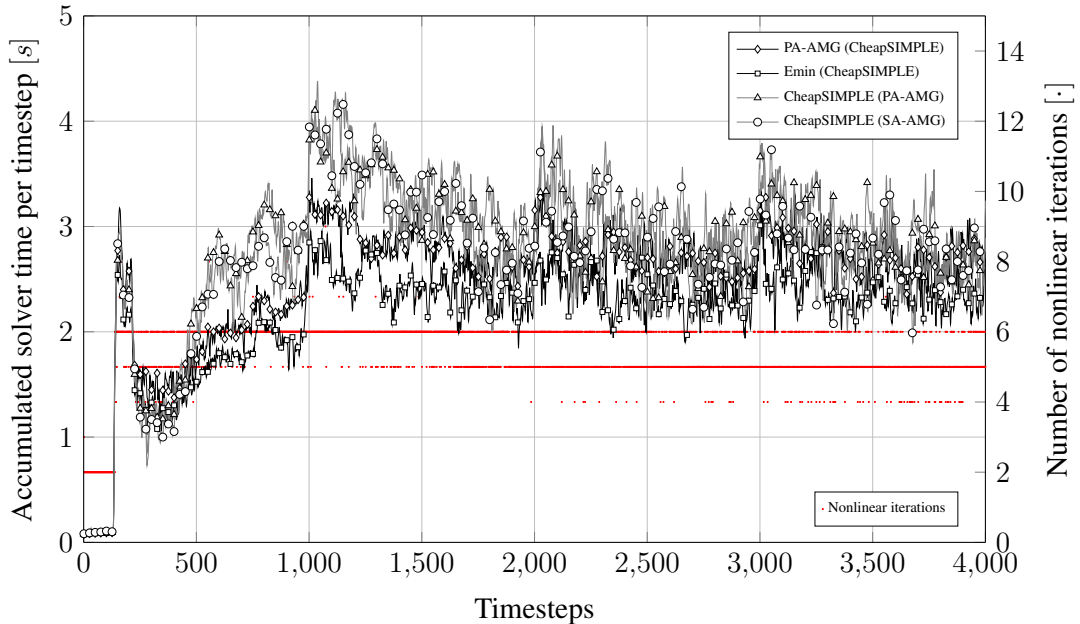
The multigrid parameters are chosen to be the same for all preconditioner variants: the minimum size of the aggregates is set to 6 nodes for the two-dimensional problem and the maximum coarse level size is set to 1000 degrees of freedom, yielding a 3 level multigrid method.

For the fully coupled AMG variants, different transfer operator strategies are compared, namely the non-smoothed (PA-AMG) transfer operators and the energy minimization approach with local damping parameters for transfer operator smoothing denoted by Emin, cf. [57]. For the nested AMG variants, we compare transfer operators based on PA-AMG and SA-AMG. All the simulations have been run on 16 cores (spread over 2 Intel Xeon E5-2670 Octocore CPUs).

Figure 7a shows the accumulated number of linear iterations in each time step. One can see that the number of linear iterations is significantly lower for the fully coupled AMG variants than with the CheapSIMPLE based methods. This can be explained by the better approximation of the displacement degrees of freedom using 3 instead of 1 damped Gauss–Seidel sweeps. Accumulated timings for the solution of each time step are reported in Figure 7b. Again, the fully coupled AMG variants perform



(a) Accumulated number of linear GMRES iterations for all nonlinear iterations per time step.



(b) Accumulated timings for the solution phase for all nonlinear iterations per time step.

Figure 7. 1000 collapsing rings example – Results for different AMG preconditioner variants.

better, although the difference is less pronounced due to the higher computational effort of fully coupled AMG implementations.

Finally, overall timings for the linear solver including preconditioner setup are reported in Table IV. Overall solver time only varies slightly for all variants. The variants Emin (CheapSIMPLE) and CheapSIMPLE (SA-AMG) need more setup time due to the additional effort of prolongator smoothing. Emin (CheapSIMPLE) can fully amortize the additional setup cost during the solve phase due to coarse grid corrections, that respect the contact constraints, while CheapSIMPLE (SA-AMG) does

Table IV. 1000 deformable rings – Exemplary timings in [s] of the different preconditioning variants from Table III for the full simulation (4000 time steps).

Method	Setup costs	Solver time	Overall solver time
PA-AMG (CheapSIMPLE)	11870	10013	21883
Emin (CheapSIMPLE)	12820	8679	21499
CheapSIMPLE (PA-AMG)	11730	11103	22833
CheapSIMPLE (SA-AMG)	12300	10763	23063

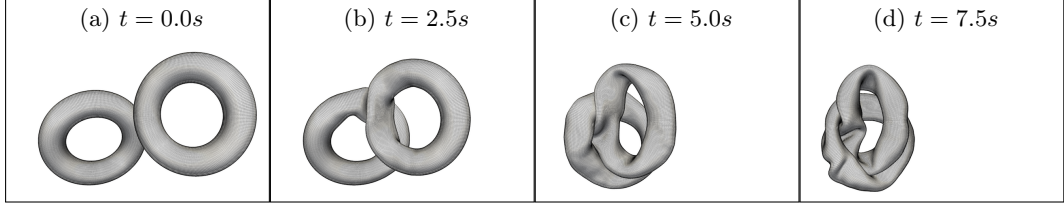


Figure 8. Two tori impact example – Characteristic stages of deformation.

not have this benefit and, thus, requires the largest overall solver time. To show a fair comparison, the preconditioner has been rebuilt in every nonlinear iteration step. Of course, re-use strategies might increase amortization of setup costs and reduce overall solver timings when solving actual problems.

### 6.3. Two tori impact example

Inspired by a similar analysis in [87], the problem setup of the two tori impact example with geometry and load conditions from [47] is used.

**6.3.1. Setup** The example consists of two thin-walled tori with a Neo-Hookean material model ( $E = 2250$ ,  $\nu = 0.3$ ,  $\rho_0 = 0.1$ ) with a major and minor radius of 76 and 24 units and a wall thickness of 4.5 units. The left torus in Figure 8 lies in the  $xy$ -plane with resting initial conditions. The right torus has been rotated around the  $y$ -axis by 45 degrees and has an initial velocity of 1.0 directed towards the left torus. The simulated time is 10s divided into 200 time steps with a time step size of 0.05s using a generalized- $\alpha$  time integration scheme [14]. The mesh consists of 284672 first-order hexahedral elements with 350208 nodes.

With the rather complex geometry and contact configuration, that heavily and frequently changes over time, this example can be considered as a representative test for the robustness and efficiency of the tested numerical methods.

**6.3.2. Stopping criteria** The stopping criteria for the semi-smooth Newton method are chosen as

$$\|\Delta \mathbf{u}\|_e < 10^{-7} \wedge \left( \left\| \frac{\mathbf{r}_i^u}{\mathbf{r}_0^u} \right\|_e < 10^{-8} \wedge \left\| \mathbf{r}_i^\lambda \right\|_e < 10^{-4} \right). \quad (27)$$

Here,  $\mathbf{r}_i^u$  and  $\mathbf{r}_i^\lambda$  denote the (nonlinear) residual for the displacement variables and Lagrange multipliers in the  $i$ -th Newton iteration, respectively. The quantity  $\Delta \mathbf{u}$  describes the solution increment for the displacement variables only.

A preconditioned GMRES solver is used with the convergence criterion

$$\left\| \frac{\mathbf{r}^k}{\mathbf{r}^0} \right\|_e < 10^{-8} \quad (28)$$

for the full residual vector  $\mathbf{r}^k = \begin{bmatrix} \mathbf{r}^u \\ \mathbf{r}^\lambda \end{bmatrix}$  in the linear iteration step  $k$ .

**6.3.3. Results** An overview of the different tested preconditioner variants is given in Table V. We study variants with the fully coupled multigrid approach, the nested multigrid approach, and a SIMPLE based variant without multigrid at all. For the fully coupled AMG variants, the transfer operators

Table V. Two tori impact example – Different AMG variants.

Full multigrid based methods	SIMPLE based methods
<b>PA-AMG (CheapSIMPLE)</b> Transfer operators: PA-AMG Level smoother: 1 CheapSIMPLEC(0.8) – Pred. smoother: 1 SGS (0.8) – Corr. smoother: ILU (0)	<b>CheapSIMPLE (SGS)</b> Transfer operators: – Block prec.: 2 CheapSIMPLEC(0.8) – Pred. smoother: 3 SGS (0.8) – Corr. smoother: ILU (0)
<b>SA-AMG (CheapSIMPLE)</b> Transfer operators: SA-AMG (0.4) Level smoother: 1 CheapSIMPLEC(0.8) – Pred. smoother: 1 SGS (0.8) – Corr. smoother: ILU (0)	<b>CheapSIMPLE (SA-AMG)</b> Block prec.: 2 CheapSIMPLEC(0.8) – Pred. smoother: AMG – Transfer op.: SA-AMG (0.4) – Level sm.: 2 SGS (0.8) – Corr. smoother: ILU (0)

Table VI. Two tori impact example – Exemplary timings in [s] of the different preconditioning variants from Table V for the full simulation over 200 time steps.

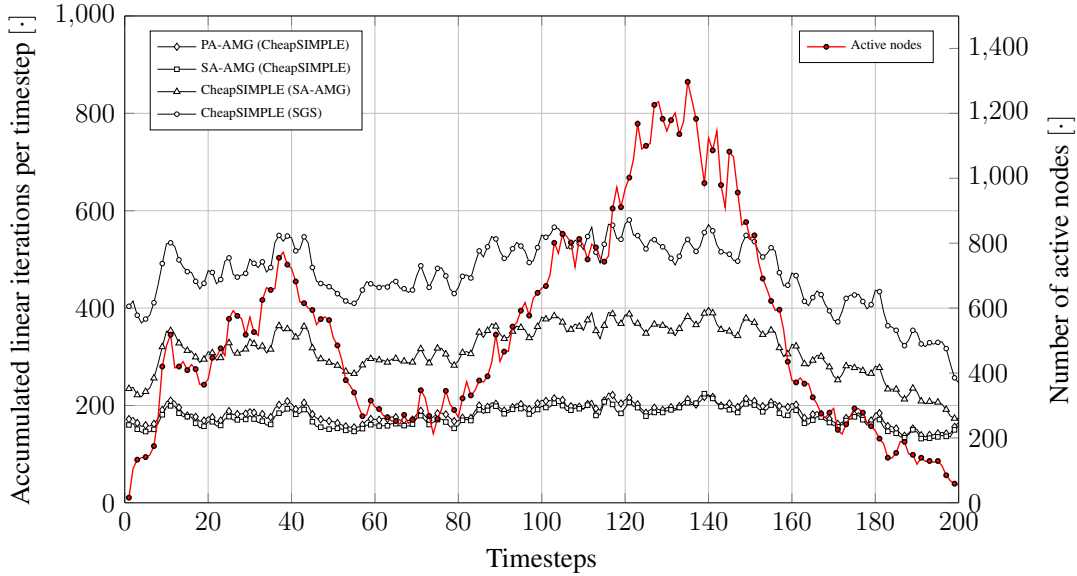
Method	Setup costs	Solver time	Overall solver time
PA-AMG (CheapSIMPLE)	11630	4658	16288
SA-AMG (CheapSIMPLE)	12250	4564	16814
CheapSIMPLE (SA-AMG)	12130	4731	16861
CheapSIMPLE (SGS)	10270	9320	19590

for the displacement blocks are varied. Particularly, non-smoothed transfer operators (PA-AMG) are compared to smoothed aggregation transfer operators (SA-AMG). All the simulations have been run on 16 cores (spread over 2 Intel Xeon E5-2670 Octocore CPUs).

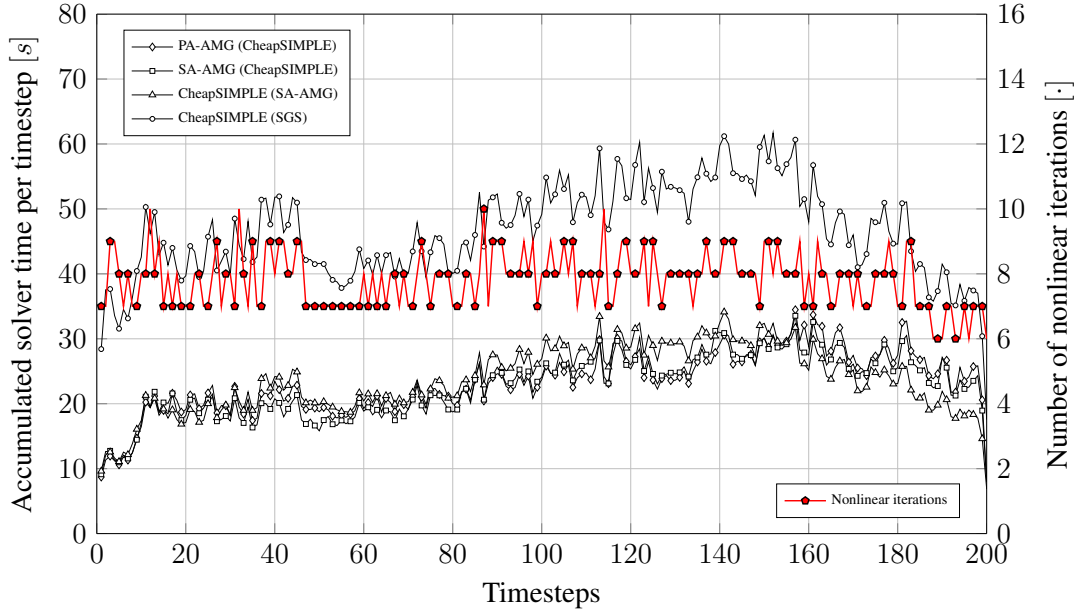
Figure 9a shows the accumulated number of iterations for solving all linear systems in one time step. Obviously, the SIMPLE based methods need more linear iterations than the AMG based methods. In this example, there is nearly no difference between the non-smoothed transfer operator variant PA-AMG (CheapSIMPLE) and the smoothed transfer operator variant SA-AMG (CheapSIMPLE). Furthermore, there is no clear and obvious correlation between the number of linear iterations and the number of active nodes. This indicates that the fully coupled multigrid method is robust and efficient with regard to the increasing complexity of the contact configuration over time, which is not the case for cheaper methods such as the SIMPLE based methods. Evidently, one can see a significant drop in the linear iterations for the last 20 time steps of the simulation, which may correspond to the small number of nodes in contact.

When looking at the corresponding solver timings over the time steps in Figure 9b, one finds the CheapSIMPLE (SA-AMG) method to be very close to the AMG based methods PA-AMG (CheapSIMPLE) and SA-AMG (CheapSIMPLE). For the AMG based methods, one sweep with a CheapSIMPLEC method is applied on each level, which internally uses one sweep with a symmetric Gauss–Seidel iteration for the primary variable and one ILU sweep for the constraint equation. That is, quite a lot of time is invested in the coupling on all levels with the comparably expensive ILU method. In contrast to the AMG based method, the CheapSIMPLE (SA-AMG) method uses 2 sweeps with a CheapSIMPLE preconditioner for the coupling (on the finest level only). Internally, a 3 level AMG multigrid is used with 2 symmetric Gauss–Seidel sweeps for the level smoother and an ILU sweep for the constraint correction equation. These parameters have been found to result in a reasonably low number of linear iterations. For this example the experiment shows that the CheapSIMPLE (SA-AMG) method needs twice as many iterations as the SA-AMG (CheapSIMPLE) method, but the costs per iteration are only half of the costs of the SA-AMG (CheapSIMPLE). Nevertheless, the AMG based methods seem to have a small advantage, when the number of nodes in contact increases.

Last but not least, the overall timings for the linear solver are reported in Table VI. Except for the CheapSIMPLE (SGS) variant, which is far away from the others, there is no clear winner. The setup costs are quite close, since the same transfer operators have to be built for all methods with only a small difference for smoothed versus non-smoothed transfer operators. To show a fair comparison, the preconditioner has been rebuilt in every nonlinear iteration step. Of course, re-use strategies might increase amortization of setup costs and reduce overall solver timings when solving actual problems.



(a) Accumulated number of linear GMRES iterations for all nonlinear iterations per timestep.



(b) Accumulated timings for the solution phase for all nonlinear iterations per timestep.

Figure 9. Two tori impact example – Results for different saddle point preconditioner variants.

## 7. CONCLUSION

We presented algebraic multigrid schemes designed for saddle point problems arising from contact problems using mortar finite element methods. The new fully coupled multigrid scheme has the advantage that the contact constraints are considered on all multigrid levels which significantly reduces the number of iterations. It gives the user full control over the coupling process by appropriately choosing the solver parameters. Additionally, we proposed a novel aggregation method for the Lagrange multipliers, which reuses existing aggregation information at the contact interface. We demonstrated

the robustness and efficiency of the overall multigrid method for large examples with increasingly complex contact configurations over time.

## REFERENCES

- [1] M. F. Adams. Algebraic multigrid methods for constrained linear systems with applications to contact problems in solid mechanics. *Numerical Linear Algebra with Applications*, 11(2-3):141–153, 2004.
- [2] F. B. Belgacem. The mortar finite element method with Lagrange multipliers. *Numerische Mathematik*, 84(2):173–197, 1999.
- [3] M. Benzi. Preconditioning techniques for large linear systems: a survey. *Journal of Computational Physics*, 182(2):418–477, 2002.
- [4] L. Berger-Vergiat, C. A. Glusa, J. J. Hu, M. Mayr, A. Prokopenko, C. M. Siefert, R. S. Tuminaro, and T. A. Wiesner. MueLu User’s Guide 2.0. Technical Report SAND2019-0537, Sandia National Laboratories, Albuquerque, NM (USA) 87185, 2019.
- [5] C. Bernardi, Y. Maday, and A. T. Patera. A new nonconforming approach to domain decomposition: The mortar element method. In H. Brezis and J. Lions, editors, *Nonlinear partial differential equations and their applications*, pages 13–51. Pitman/Wiley: London/New York, 1994.
- [6] J. Bonari, M. R. Marulli, N. Hagemeyer, M. Mayr, A. Popp, and M. Paggi. A multi-scale FEM-BEM formulation for contact mechanics between rough surfaces. *Computational Mechanics*, published online.
- [7] D. Braess and R. Sarazin. An efficient smoother for the stokes problem. *Applied Numerical Mathematics*, 23:3–19, 1997.
- [8] D. Braess, M. Dryja, and W. Hackbusch. A multigrid method for nonconforming FE-discretisations with application to non-matching grids. *Computing*, 63(1):1–25, 1999.
- [9] D. Braess and W. Dahmen. Stability estimates of the mortar finite element method for 3-dimensional problems. *East-West Journal of Numerical Mathematics*, 6:249–264, 1998.
- [10] D. Braess, W. Dahmen, and C. Wiener. A multigrid algorithm for the mortar finite element method. *SIAM Journal on Numerical Analysis*, 37(1):pp. 48–69, 2000.
- [11] J. H. Bramble, J. E. Pasciak, and A. T. Vassilev. Analysis of the inexact uzawa algorithm for saddle point problems. *SIAM Journal on Numerical Analysis*, 34(3):pp. 1072–1092, 1997.
- [12] F. J. Cavalieri and A. Cardona. Three-dimensional numerical solution for wear prediction using a mortar contact algorithm. *International Journal for Numerical Methods in Engineering*, 96(8):467–486, 2013.
- [13] P. W. Christensen, A. Klarbring, J. S. Pang, and N. Strömberg. Formulation and comparison of algorithms for frictional contact problems. *International Journal for Numerical Methods in Engineering*, 42(1):145–173, 1998.
- [14] J. Chung and G. Hulbert. A Time Integration Algorithm for Structural Dynamics With Improved Numerical Dissipation: The Generalized- $\alpha$  Method. *Journal of Applied Mechanics*, 60(2):371–375, 1993.
- [15] C. Danowski, V. Gravemeier, L. Yoshihara, and W. A. Wall. A monolithic computational approach to thermo-structure interaction. *International Journal for Numerical Methods in Engineering*, 95(13):1053–1078, 2013.
- [16] L. De Lorenzis, I. Temizer, P. Wriggers, and G. Zavarise. A large deformation frictional contact formulation using NURBS-based isogeometric analysis. *International Journal for Numerical Methods in Engineering*, 87(13):1278–1300, 2011.
- [17] L. De Lorenzis, P. Wriggers, and T. J. Hughes. Isogeometric contact: a review. *GAMM-Mitteilungen*, 37(1):85–123, 2014.
- [18] H. Elman, V. E. Howle, J. Shadid, R. Shuttleworth, and R. Tuminaro. A taxonomy and comparison of parallel block multi-level preconditioners for the incompressible Navier-Stokes equations. *Journal of Computational Physics*, 227(3):1790–1808, January 2008.
- [19] H. C. Elman and G. H. Golub. Inexact and preconditioned Uzawa algorithms for saddle point problems. *SIAM Journal on Numerical Analysis*, 31(6):pp. 1645–1661, 1994.
- [20] P. Farah, W. A. Wall, and A. Popp. An implicit finite wear contact formulation based on dual mortar methods. *International Journal for Numerical Methods in Engineering*, 111(4):325–353, 2016.
- [21] M. Franke, C. Hesch, and P. Betsch. An augmentation technique for large deformation frictional contact problems. *International Journal for Numerical Methods in Engineering*, pages –, 2013.
- [22] M. W. Gee, J. J. Hu, and R. S. Tuminaro. A new smoothed aggregation multigrid method for anisotropic problems. *Numerical Linear Algebra with Applications*, 16:19–37, 2009.
- [23] M. W. Gee, U. Kättler, and W. A. Wall. Truly monolithic algebraic multigrid for fluid–structure interaction. *International Journal for Numerical Methods in Engineering*, 85(8):987–1016, 2011.
- [24] M. Gitterle, A. Popp, M. W. Gee, and W. A. Wall. Finite deformation frictional mortar contact using a semi-smooth Newton method with consistent linearization. *International Journal for Numerical Methods in Engineering*, 84(5):543–571, 2010.
- [25] J. Gopalakrishnan and J. E. Pasciak. Multigrid for the mortar finite element method. *SIAM Journal on Numerical Analysis*, 37(3):1029–1052, 2000.
- [26] M. Griebel, T. Neunhoeffer, and H. Regler. Algebraic multigrid methods for the solution of the Navier–Stokes equations in complicated geometries. *International Journal for Numerical Methods in Fluids*, 26(3):281–301, 1998.
- [27] W. Hackbusch. *Iterative Solution of Large Sparse Systems of Equations*, volume 95 of *Applied Mathematical Sciences*. Springer, 1994.
- [28] W. Hackbusch. *Multi-Grid Methods and Applications*, volume 4 of *Series in Computational Mathematics*. Springer, 1st edition edition, 1985.

- [29] S. Hartmann, S. Brunssen, E. Ramm, and B. I. Wohlmuth. Unilateral non-linear dynamic contact of thin-walled structures using a primal-dual active set strategy. *International Journal for Numerical Methods in Engineering*, 70(8):883–912, 2007.
- [30] M. Hiermeier, W. A. Wall, and A. Popp. A truly variationally consistent and symmetric mortar-based contact formulation for finite deformation solid mechanics. *Computer Methods in Applied Mechanics and Engineering*, 342:532–560, 2018.
- [31] M. Hintermüller, K. Ito, and K. Kunisch. The primal-dual active set strategy as a semi-smooth Newton method. *SIAM Journal on Optimization*, 13(3):865–888, 2002.
- [32] S. Hüeber and B. I. Wohlmuth. A primal-dual active set strategy for non-linear multibody contact problems. *Computer Methods in Applied Mechanics and Engineering*, 194(27-29):3147–3166, 2005.
- [33] S. Hüeber, G. Stadler, and B. I. Wohlmuth. A primal-dual active set algorithm for three-dimensional contact problems with Coulomb friction. *SIAM Journal on Scientific Computing*, 30(2):572–596, 2008.
- [34] A. Janka. Smoothed aggregation multigrid for a Stokes problem. *Computing and Visualization in Science*, 11(3):169–180, 2008.
- [35] C. Keller, N. I. M. Gould, and A. J. Wathen. Constrained preconditioning for indefinite linear systems. *SIAM Journal on Matrix Analysis & Applications*, 21(4):1300 – 1317, 2000.
- [36] R. H. Krause and B. I. Wohlmuth. Multigrid methods for mortar finite elements. In *Multigrid methods, VI (Gent, 1999)*, volume 14 of *Lecture Notes in Computational Science and Engineering*, pages 136–142. Springer, Berlin, 2000.
- [37] B. P. Lamichhane, R. P. Stevenson, and B. I. Wohlmuth. Higher order mortar finite element methods in 3D with dual Lagrange multiplier bases. *Numerische Mathematik*, 102(1):93–121, 2005.
- [38] U. Langer and H. Yang. Numerical Simulation of Fluid–Structure Interaction Problems with Hyperelastic Models: A Monolithic Approach. *Mathematics and Computers in Simulation*, 145:186–208, 2018.
- [39] J. Lengiewicz and S. Stupkiewicz. Continuum framework for finite element modelling of finite wear. *Computer Methods in Applied Mechanics and Engineering*, 205-208:178–188, 2012.
- [40] Q. Li and V. L. Popov. Adhesive contact between a rigid body of arbitrary shape and a thin elastic coating. *Acta Mechanica*, 230(7):2447–2453, 2019.
- [41] R. Lonsdale. *An algebraic multigrid scheme for solving the Navier-Stokes equations on unstructured meshes*, volume 7 of *Numerical Methods in Laminar and Turbulent Flow*, pages 1432–1442. Pineridge press, Swansea, U.K., 1991.
- [42] E. Milanesi, T. Brink, R. Aghababaei, and J.-F. Molinari. Emergence of self-affine surfaces during adhesive wear. *Nature Communications*, 10(1116), 2019.
- [43] Y. Notay. A new analysis of block preconditioners for saddle point problems. *SIAM Journal on Matrix Analysis and Applications*, 35(1):143–173, 2014.
- [44] S. V. Patankar and D. B. Spalding. A calculation procedure for heat, mass and momentum transfer in three-dimensional parabolic flows. *International Journal of Heat and Mass Transfer*, 15:1787–1972, 1972.
- [45] S. V. Patankar. *Numerical Heat Transfer and Fluid Flow*. Hemisphere Publishing Corporation, New York, 1980.
- [46] V. L. Popov. *Contact Mechanics and Friction: Physical Principles and Applications*. Springer, Berlin, 2nd edition, 2017.
- [47] A. Popp. *Mortar Methods for Computational Contact Mechanics and General interface Problems*. PhD thesis, Technische Universität München, 2012.
- [48] A. Popp, M. Gitterle, M. W. Gee, and W. A. Wall. A dual mortar approach for 3D finite deformation contact with consistent linearization. *International Journal for Numerical Methods in Engineering*, 83 (11):1428–1465, 2010.
- [49] A. Popp, B. I. Wohlmuth, M. W. Gee, and W. A. Wall. Dual quadratic mortar finite element methods for 3D finite deformation contact. *SIAM Journal on Scientific Computing*, 34:B421–B446, 2012.
- [50] A. Popp, M. W. Gee, and W. A. Wall. A finite deformation mortar contact formulation using a primal–dual active set strategy. *International Journal for Numerical Methods in Engineering*, 79 (11):1354–1391, 2009.
- [51] A. Popp, A. Seitz, M. W. Gee, and W. A. Wall. Improved robustness and consistency of 3D contact algorithms based on a dual mortar approach. *Computer Methods in Applied Mechanics and Engineering*, 264:67–80, 2013.
- [52] M. A. Puso and T. A. Laursen. A mortar segment-to-segment contact method for large deformation solid mechanics. *Computer Methods in Applied Mechanics and Engineering*, 193(6-8):601–629, 2004.
- [53] M. A. Puso and T. A. Laursen. A mortar segment-to-segment frictional contact method for large deformations. *Computer Methods in Applied Mechanics and Engineering*, 193(45-47):4891–4913, 2004.
- [54] L. Qi and J. Sun. A nonsmooth version of Newton’s method. *Mathematical Programming*, 58(1):353–367, 1993.
- [55] Y. Saad and M. Schultz. GMRES: A generalized minimal residual algorithm for solving nonsymmetric linear systems. *SIAM Journal on Scientific and Statistical Computing*, 7(3):856–869, 1986.
- [56] Y. Saad. *Iterative Methods for Sparse Linear Systems*. SIAM, second edition edition, 2003.
- [57] M. Sala and R. S. Tuminaro. A new Petrov-Galerkin smoothed aggregation preconditioner for nonsymmetric linear systems. *SIAM Journal on Scientific Computing*, 31(1):143–166, 2008.
- [58] R. A. Sauer. Enriched contact finite elements for stable peeling computations. *International Journal for Numerical Methods in Engineering*, 87(6):593–616, 2011.
- [59] A. Seitz, A. Popp, and W. A. Wall. A semi-smooth newton method for orthotropic plasticity and frictional contact at finite strains. *Computer Methods in Applied Mechanics and Engineering*, 285(0):228–254, 2015.
- [60] A. Seitz, P. Farah, J. Kremheller, B. I. Wohlmuth, W. A. Wall, and A. Popp. Isogeometric dual mortar methods for computational contact mechanics. *Computer Methods in Applied Mechanics and Engineering*, 301:259–280, 2016.

- [61] K. Stüben. *Multigrid*, Appendix A: An introduction to algebraic multigrid, pages 413–533. U. Trottenberg and C.W. Oosterlee and A. Schüller, 2001.
- [62] I. Temizer, P. Wriggers, and T. J. R. Hughes. Contact treatment in isogeometric analysis with NURBS. *Computer Methods in Applied Mechanics and Engineering*, 200(9–12):1100–1112, 2011.
- [63] I. Temizer, P. Wriggers, and T. J. R. Hughes. Three-dimensional mortar-based frictional contact treatment in isogeometric analysis with NURBS. *Computer Methods in Applied Mechanics and Engineering*, 209–212(0):115–128, 2012.
- [64] T. E. Tezduyar, S. Sathe, and K. Stein. Solution techniques for the fully discretized equations in computation of fluid–structure interactions with the space–time formulations. *Computer Methods in Applied Mechanics and Engineering*, 195(41–43):5743–5753, 2006.
- [65] U. Trottenberg, C. Oosterlee, and A. Schüller. *Multigrid*. Academic Press, 2001. ISBN 9780127010700.
- [66] A. I. Vakis, V. A. Yastrebov, J. Scheibert, L. Nicola, D. Dini, C. Minfray, A. Almqvist, M. Paggi, S. Lee, G. Limbert, J.-F. Molinari, G. Anciaux, R. Aghababaei, S. Echeverri Restrepo, A. Papangelo, A. Cammarata, P. Nicolini, C. Putignano, G. Carbone, S. Stupkiewicz, J. Lengiewicz, G. Costagliola, F. Bosia, R. Guarino, N. M. Pugno, M. H. Müser, and M. Ciavarella. Modeling and simulation in tribology across scales: An overview. *Tribology International*, 125:169–199, 2018.
- [67] J. Van Doormaal and G. Raithby. Enhancements of the simple method for predicting incompressible fluid flows. *Numerical heat transfer*, 7(2):147–163, 1984.
- [68] P. Vaněk, J. Mandel, and M. Brezina. Algebraic multigrid by smoothed aggregation for second and fourth order elliptic problems. *Computing*, 56:179–196, 1996.
- [69] P. Vaněk. Acceleration of convergence of a two-level algorithm by smoothing transfer operators. *Applications of Mathematics*, 37:265–274, 1992.
- [70] P. Vaněk, J. Mandel, and M. Brezina. Algebraic multigrid on unstructured meshes. Technical report, University of Colorado at Denver, 1994.
- [71] P. Vaněk, A. Janka, and H. Guillard. Convergence of algebraic multigrid based on smoothed aggregation ii: Extension to a Petrov–Galerkin method. *INRIA Technical Report 3683*, 1999.
- [72] P. Vaněk, M. Brezina, and J. Mandel. Convergence of algebraic multigrid based on smoothed aggregation. *Numerische Mathematik*, 88:559–579, 2001.
- [73] F. Verdugo and W. A. Wall. Unified computational framework for the efficient solution of  $n$ -field coupled problems with monolithic schemes. *Computer Methods in Applied Mechanics and Engineering*, 310:335–366, 2016.
- [74] M. Wabro. Coupled algebraic multigrid methods for the Oseen problem. *Computing and Visualization in Science*, 7:141–151, 2004.
- [75] C. Wieners and B. Wohlmuth. Duality estimates and multigrid analysis for saddle point problems arising from mortar discretizations. *SIAM Journal on Scientific Computing*, 24:2163–2184, 2003.
- [76] C. Wieners and B. Wohlmuth. A general framework for multigrid methods for mortar finite elements. Technical Report 415, Universität Augsburg, Institut für Mathematik, 1999.
- [77] T. A. Wiesner, M. W. Gee, A. Prokopenko, and J. Hu. The MueLu Tutorial. Technical report, Sandia National Laboratories, 2014.
- [78] T. A. Wiesner, A. Popp, M. W. Gee, and W. A. Wall. Algebraic multigrid methods for dual mortar finite element formulations in contact mechanics. *International Journal for Numerical Methods in Engineering*, 144(4):399–430, 2018.
- [79] B. Wohlmuth. A multigrid methods for saddlepoint problems arising from mortar finite element discretizations. *ETNA. Electronic Transactions on Numerical Analysis*, 11:43–54, 2000.
- [80] B. Wohlmuth. *Discretization Techniques and Iterative Solvers Based on Domain Decomposition*, volume 17. Springer, Heidelberg, 2001.
- [81] B. I. Wohlmuth. A mortar finite element method using dual spaces for the Lagrange multiplier. *SIAM Journal on Numerical Analysis*, 38(3):989–1012, 2000.
- [82] B. I. Wohlmuth. Variationally consistent discretization schemes and numerical algorithms for contact problems. *Acta Numerica*, 20:569–734, 2011.
- [83] B. I. Wohlmuth, A. Popp, M. W. Gee, and W. A. Wall. An abstract framework for a priori estimates for contact problems in 3D with quadratic finite elements. *Computational Mechanics*, 49:735–747, 2012.
- [84] B. Wohlmuth and R. Krause. Multigrid methods based on the unconstrained product space for mortar finite element discretizations. *SIAM Journal on Numerical Analysis*, 39:192–213, 2001.
- [85] P. Wriggers. *Computational contact mechanics*. Springer-Verlag Berlin Heidelberg, 2006.
- [86] L. Wunderlich, A. Seitz, M. D. Alaydin, B. I. Wohlmuth, and A. Popp. Biorthogonal splines for optimal weak patch-coupling in isogeometric analysis with applications to finite deformation elasticity. *Computer Methods in Applied Mechanics and Engineering*, 346:197–215, 2019.
- [87] B. Yang and T. Laursen. A contact searching algorithm including bounding volume trees applied to finite sliding mortar formulations. *Computational Mechanics*, 41(2):189–205, 2008.
- [88] O. C. Zienkiewicz, R. L. Taylor, and D. D. Fox. *The Finite Element Method for Solid and Structural Mechanics*. Butterworth-Heinemann, Oxford, 7th edition, 2014.
- [89] W. Zulehner. A class of smoothers for saddle point problems. *Computing*, 65:227–246, 2000.
- [90] W. Zulehner. Analysis of iterative methods for saddle point problems: A unified approach. *Mathematics of Computation*, 71:479–505, 2002.